EPRI | ELECTRIC POWER RESEARCH INSTITUTE

Development of Code to Predict Stress Corrosion Cracking and Corrosion Fatigue of Low Pressure Turbine Components

Electrochemical and Corrosion Properties of Turbine Steels

Technical Report

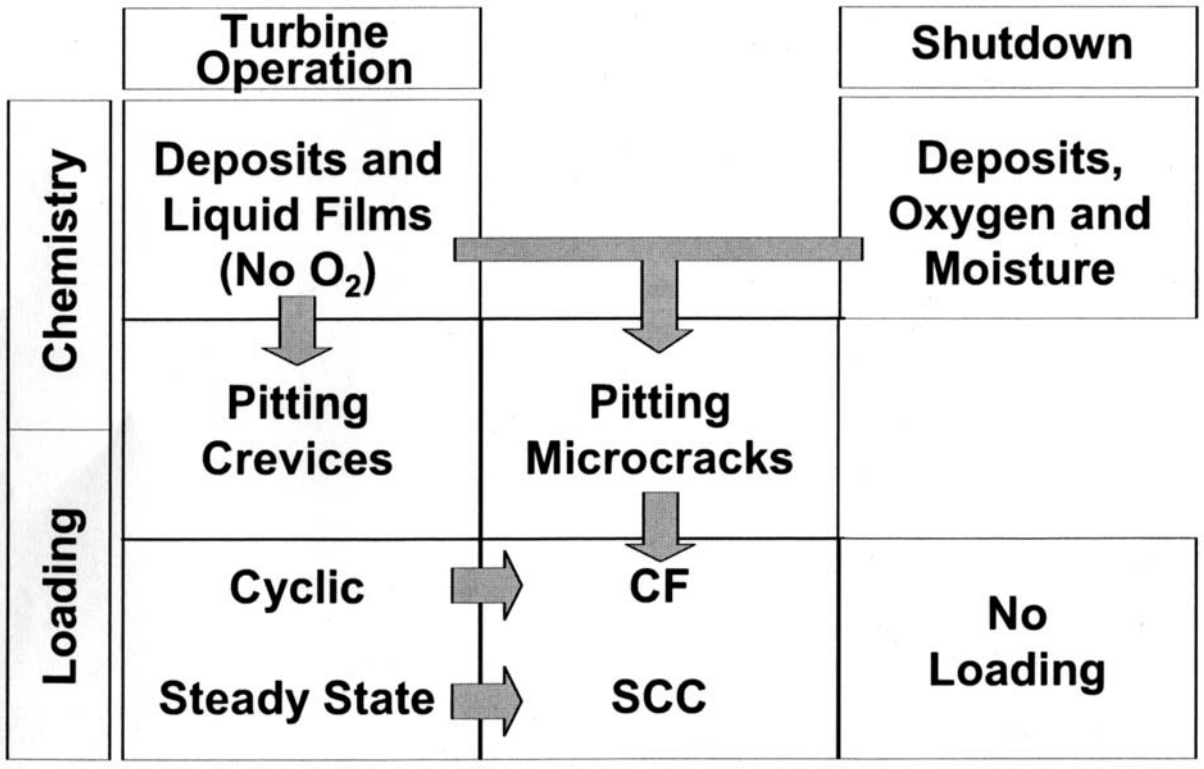

Development of Code to Predict Stress Corrosion Cracking and Corrosion Fatigue of Low Pressure Turbine Components

Electrochemical and Corrosion Properties of Turbine Steels

1010184

Final Report, December 2005

EPRI Project Managers
R. B. Dooley
S. Hesler

ELECTRIC POWER RESEARCH INSTITUTE
3420 Hillview Avenue, Palo Alto, California 94304-1395 ▪ PO Box 10412, Palo Alto, California 94303-0813 ▪ USA
800.313.3774 ▪ 650.855.2121 ▪ askepri@epri.com ▪ www.epri.com

DISCLAIMER OF WARRANTIES AND LIMITATION OF LIABILITIES

THIS DOCUMENT WAS PREPARED BY THE ORGANIZATION(S) NAMED BELOW AS AN ACCOUNT OF WORK SPONSORED OR COSPONSORED BY THE ELECTRIC POWER RESEARCH INSTITUTE, INC. (EPRI). NEITHER EPRI, ANY MEMBER OF EPRI, ANY COSPONSOR, THE ORGANIZATION(S) BELOW, NOR ANY PERSON ACTING ON BEHALF OF ANY OF THEM:

(A) MAKES ANY WARRANTY OR REPRESENTATION WHATSOEVER, EXPRESS OR IMPLIED, (I) WITH RESPECT TO THE USE OF ANY INFORMATION, APPARATUS, METHOD, PROCESS, OR SIMILAR ITEM DISCLOSED IN THIS DOCUMENT, INCLUDING MERCHANTABILITY AND FITNESS FOR A PARTICULAR PURPOSE, OR (II) THAT SUCH USE DOES NOT INFRINGE ON OR INTERFERE WITH PRIVATELY OWNED RIGHTS, INCLUDING ANY PARTY'S INTELLECTUAL PROPERTY, OR (III) THAT THIS DOCUMENT IS SUITABLE TO ANY PARTICULAR USER'S CIRCUMSTANCE; OR

(B) ASSUMES RESPONSIBILITY FOR ANY DAMAGES OR OTHER LIABILITY WHATSOEVER (INCLUDING ANY CONSEQUENTIAL DAMAGES, EVEN IF EPRI OR ANY EPRI REPRESENTATIVE HAS BEEN ADVISED OF THE POSSIBILITY OF SUCH DAMAGES) RESULTING FROM YOUR SELECTION OR USE OF THIS DOCUMENT OR ANY INFORMATION, APPARATUS, METHOD, PROCESS, OR SIMILAR ITEM DISCLOSED IN THIS DOCUMENT.

ORGANIZATION(S) THAT PREPARED THIS DOCUMENT

OLI Systems, Inc.

Pennsylvania State University

Frumkin Institute of Physical Chemistry and Electrochemistry

NOTE

For further information about EPRI, call the EPRI Customer Assistance Center at 800.313.3774 or e-mail askepri@epri.com.

CITATIONS

This report was prepared by

OLI Systems, Inc.
108 American Road
Morris Plains, NJ 07950

Principal Investigator
G. Engelhardt

Pennsylvania State University
201 Steidle Building
University Park, PA 16802

Principal Investigator
D. Macdonald

Frumkin Institute of Physical Chemistry and Electrochemistry
Russian Academy of Sciences
Leninskii Prospect 31
Moscow, Russia

Principal Investigator
A. Davydov

This report describes research sponsored by the Electric Power Research Institute (EPRI).

The report is a corporate document that should be cited in the literature in the following manner:

Development of Code to Predict Stress Corrosion Cracking and Corrosion Fatigue of Low Pressure Turbine Components: Electrochemical and Corrosion Properties of Turbine Steels. EPRI, Palo Alto, CA: 2005. 1010184.

PRODUCT DESCRIPTION

Most outage hours for steam turbines are due to corrosion of low pressure (LP) blades and disks in the phase transition zone (PTZ). Developing an effective localized corrosion damage prediction model is essential for successfully avoiding unscheduled outages of steam turbines. This report provides the initial electrochemical data needed for the model development.

Results and Findings

Key results of the experimental stage of the ongoing work can be summarized as follows:

- The general theoretical basis for the damage function analysis has been developed further to describe the different corrosion events of active and passive pit growth, development of cracks, and growth of stress corrosion and corrosion fatigue cracks.
- The quantitative characterization of the principal partial corrosion reactions on two low pressure steam turbine materials has been completed.
- The kinetic equations for hydrogen evolution and oxygen reduction have been developed.
- The experimental data has indicated an order of resistance to pitting of three common PTZ materials: 17-4PH, 403SS, and A470/471.

Challenges and Objectives

The overall work represents a major new approach to understanding and controlling corrosion in the PTZ. For the first time, a mechanistic/deterministic description of all stages in the propagation of corrosion damage has been developed. The evolution of damage can now be described by the damage functions. The remaining challenge in developing the model is to describe the evolutionary history of the local environment, the stress, and the operation.

Applications, Values, and Use

Cycle chemistry and stress effects are most often longer term for damage and failures in the PTZ of the steam turbine. Failures still occur despite much laboratory and field study. Results of this work will finally provide the needed understanding of the key PTZ processes and, thus, the means for better failure analysis. More importantly, the project results will be used in the predictive model that can be used across the turbine fleet.

EPRI Perspective

It is over 25 years since research was initiated to improve understanding of processes in the so-called thermodynamic salt zone, deposit buildup and behavior in the PTZ, and how these factors influence the major corrosion mechanisms. However, it is clear that the results of this research did not lead to a marked improvement in the overall reliability statistics of steam turbines.

Development of this model represents the first step in bringing together all the latest EPRI Strategic Science & Technology (SS&T) information on the PTZ, particularly the presence of liquid films during operation that have potential and conductivity, but contain no oxygen. The model also has confirmed the effects of unit operation and clearly shows that pitting and corrosion damage is initiated during unprotected shutdown conditions. Reliable electrochemical data for oxygen, hydrogen, and water reduction—along with values for the passive corrosion current density—have now been determined in this parallel EPRI research. The next step will be to test the model on real corrosion situations. Ultimately, an EPRI code for corrosion fatigue and stress corrosion cracking of LP turbine components will be developed.

Approach

The project team used a rotating disk electrode to determine the current density versus potential curves for the PTZ materials. The teams determined the corrosion potential and corrosion currents characterizing dissolution in a pit from the Tafel portions of the anodic and cathodic polarization curves. They also used visual and microscopic examination of the material surfaces to quantify the pitting phenomena.

Keywords

Power plant availability
Steam turbines
Steam chemistry
Corrosion
Electrochemistry

ABSTRACT

This report provides a technical update to EPRI reports (1004190 and 1009690) published in 2004 and 2005. In those reports, a deterministic model based on Damage Function Analysis for predicting localized corrosion damage in low pressure steam turbines was developed, and model computer simulations for probability of failure were performed. However, as emphasized in those reports, the actual deterministic prediction of the propagation of corrosion damage in real turbines requires information about kinetic (electrochemical) parameters of the particular turbine steels of interest under the appropriate environmental conditions. The current report is devoted to the experimental measurements of those parameters for the steels of interest (403SS, A470/471, 17-4PH, and 20Kh13). The data have been expressed in analytical form, so that they can be easily incorporated into computer codes.

Kinetic parameters for the principal cathodic reactions occurring in the corrosion processes have been measured. These reactions are the reduction of dissolved oxygen and hydrogen evolution. The kinetic parameters have been measured for A470/471 and 403SS in NaCl solutions having various NaCl concentrations, pHs, temperatures, and dissolved oxygen concentrations. The dependences of the current density for oxygen reduction on the dissolved oxygen concentration at temperatures ranging from 20°C to 95°C and on the pH of solution are determined. The kinetic equations of oxygen reduction relating the process rate (the current density) to the overpotential of the reaction are also obtained. The kinetic equations for the hydrogen evolution process, which proceeds according to two mechanisms—the discharge of hydroxonium ions and the discharge of water molecules—are obtained. The ranges of pH values where the hydrogen evolution proceeds by each of these mechanisms are determined.

It is shown that the corrosion potential of both steels varies with time as pitting corrosion develops, indicating that the corrosion rates of the steels also vary with time. The anodic and cathodic polarization curves on the electrodes totally activated with chloride ions are obtained. Using these data, the corrosion potential and the current density of steel dissolution in the pits are estimated. The pH value of the solution and the concentration of dissolved oxygen are the two parameters that have the strongest effect on the corrosion current in a pit. The corrosion current density decreases by more than an order of magnitude with an increase in the pH value from 2 to 10 and with a decrease in the concentration of oxygen from 10^{-6} mol/cm^3 (oxygen atmosphere) to 10^{-8} mol/cm^3 (argon atmosphere).

From a comparison of the experimental data, it is concluded that steel 17-4PH exhibits the highest resistance to pitting corrosion in the NaCl solutions, 403SS and 20Kh13 exhibit somewhat lower resistance, and A470/471 is much less resistant to this form of localized corrosion.

Using computer processing of the experimental data, equations predicting the corrosion potential and corrosion current density as a function of temperature, pH, and chloride and oxygen concentrations have been obtained. These equations are now being implemented in previously developed models and computer codes for prediction of the corrosion damage in LP steam turbines.

CONTENTS

LIST OF FIGURES

LIST OF TABLES

1
INTRODUCTION AND OBJECTIVES

Localized corrosion damage in low pressure steam turbine components is often considered as the main cause of turbine unavailability [1, 2]. The principal objective of this project is to develop methods for predicting the evolution of corrosion damage (pitting, stress corrosion cracking, and corrosion fatigue) in steam turbine blades and discs. The development of such methods is essential for the avoidance of unscheduled downtime in steam turbines and, in some cases, also for devising effective strategies for extending the turbine service life.

In the previous report and articles [3-5] the general models and computer codes for predicting probability of failure in steam turbines have been described. These models can predict corrosion damage, (e.g. probability of failure, P_f, as a function of critical crack depth, L_{cr}, and service life, t_s) if external conditions are known as a function of time in real systems. In this case, detailed information about the kinetic parameters for various chemical and electrochemical processes occurring in the system (for example, exchange current densities and transfer coefficients for the various charge transfer reactions) is necessary. These models can also be used in the case when the depth of the deepest crack (pit) is known as a function of time in turbines under practical conditions from short-time experiments. In this latter case the extrapolation of corrosion damage with time can be done, in principle, without any information about the kinetic coefficients of the system. However, even in this case, the information about kinetic coefficients is desirable. Thus, knowledge of the kinetic parameters can reduce the number of unknown parameters that must be determined by optimization and can therefore increase the accuracy of the prediction. On the other hand this information allows prediction of corrosion damage when external (operation) conditions can change. In all cases, it is necessary to specify the corrosion evolutionary path in terms of the evolution of those properties of the system (e.g., temperature, pH, and oxygen concentration) that have an impact on the rate of corrosion.

This report presents the results of experimental investigations of electrochemical behavior of stainless steels that are widely used in low pressure steam turbines. The kinetic properties of the cathodic and anodic processes of the components that combine to form the overall corrosion process were studied at various concentrations, temperatures, and pH values of NaCl solutions containing various amounts of dissolved oxygen. Anodic and cathodic voltammograms, which were measured by a special procedure, were used to determine the current density of steel dissolution in pits and the corrosion potential under various conditions. The long-term corrosion potential measurements (the “open-circuit potentials”) were performed, and the corrosion damage of test specimens was analyzed after holding them in the NaCl solutions for prescribed times. Measured electrochemical parameters, along with the measured dependences of corrosion potential, E_{corr} and corrosion currents as a function of external conditions, can be used in the models and computer codes for predicting corrosion damage.

Table 1-1 lists the compositions of the 403SS and A470 steel used in this study. The most significant difference between them is that 403SS contains a considerably larger amount of chromium, which commonly has a pronounced effect on the electrochemical behavior of steels. Table 1-1 also lists the compositions of two other steels, 20Kh13 and 17-4 PH, which are used for the production of steam turbine components, since several experiments were performed to study the electrochemical and corrosion behavior of these steels, in order to compare them with the behavior of A470 and 403SS.

In this report, only some of the data obtained on the electrochemical and corrosion behavior of several of the steels are presented. The additional results will be presented in a later report and after additional analysis to extract system property information more fully in several papers, which are in preparation.

Table 1-1
Chemical Compositions of Tested Steels

	403SS	A470/471	17-4PH	20Kh13
C	0.12	0.25-0.30	0.04	0.205
Ni	0.22	0.9-1.2	3.00-5.00	0.20
Cr	12.34	1.7-2.0	15.00-17.00	12.45
Mo	0.15	0.6-0.8	0.500	0.1
V	-	0-0.06	-	-
Mn	0.42	0.5-0.8	1.00	0.32
Si	0.18	0-0.30	1.00	0.41
Co	0.05	-	-	-
Cu	0.05	-	3.00-5.00	-
Sn	0.004	-	-	-
Al	0.01	-	-	-
N	0.03	-	-	-
S	0.04	0-0.015	0.03	0.009
P	0.020	0-0.01	0.04	0.014
Nb	-	-	0.400	-
Ti	-	-	0.150	-
Fe	balance	balance	balance	balance

2
EXPERIMENTAL TECHNIQUE AND RESULTS

The current density vs. the potential curves (voltammograms) for the steels were measured using the potentiodynamic method with a potential scan rate of 1 mV/s. A rotating disk electrode was used. To determine the kinetic parameters of metal anodic dissolution in a pit, the direct potentiodynamic curve was measured from the open-circuit potential to the pitting potential, or somewhat higher; the electrode was held at this potential up to the total activation of the entire electrode surface. Then, the reverse potentiodynamic curve was measured to the potential at which the current sign changed, and then, the potentiodynamic curve was measured further into the cathodic range. The portion of reverse anodic potentiodynamic curve in the range of rather low current densities (in order to avoid ohmic potential drop error in the measurement) was plotted with semilogarithmic coordinates. The cathodic portion of potentiodynamic curve was also plotted with semilogarithmic coordinates. In the cases where activation of the entire surface of the test specimen with chloride ion was hampered (for example, at relatively low concentrations of NaCl), specially selected modes of pulse surface activation were used. The determination of corrosion potential and corrosion current characterizing dissolution in a pit from the Tafel portions of the anodic and cathodic polarization curves will be described in the corresponding section.

The direct measurements of the steel corrosion potential in the NaCl solutions of various concentrations and pH values were performed by holding the test specimens in the corrosive medium for a long time (up to 3000 hours). Visual and microscopic examinations of steel specimen surfaces were performed upon termination of each experiment.

The electrochemical cells used enabled the researchers to perform measurements at prescribed temperatures while saturating the solution with air, argon, or oxygen. The potentials were measured against a saturated silver-chloride reference electrode. In the text and figures, the potentials are given with respect to a standard hydrogen electrode.

2.1 Longterm Measurements of Corrosion Potential

2.1.1 Steel 403SS

Figures 2-1 and 2-2 give the results of longterm measurements of the corrosion potential, E_{corr}, of 403SS in the NaCl solutions of several concentrations ranging from 0.001 to 1.0 M and in 0.1 M NaCl solution at pH 2, 6, and 10. The values of E_{corr} in the more concentrated solutions (from 0.1 to 1.0 M) decrease with the time of specimen exposure in the solutions and reach approximately –0.2 to –0.24 V at the end of the test period of 3000 h. A shift of potential in the negative direction with time is associated with the development of pitting, as a result of the predominant

action of aggressive chloride ions inducing passivity breakdown on the steel surface. In more dilute solutions (0.01 and 0.001 M), E_{corr} shifts to more positive values, due to the predominant passivation process as a result of interaction of the metal with oxygen and/or water. At the end of the measurement period, E_{corr} of 403SS is approximately 0.1 V in the 0.01 M NaCl solution and is approximately 0.15 V in the 0.001 M NaCl solution. However, this does not mean that the steel is immune to pitting corrosion in these solutions. Pitting, which results from the breakdown of passivity, can occur after a longer period of time, because the breakdown process is characterized by an induction time that is a function of potential, [Cl^-], pH, temperature, and so on. Thus, it is well known that the induction period for stable pitting increases and the pitting rate decreases with a decrease in the concentration of aggressive solution. The results of examination of steel specimen surfaces after longterm (two or more months) exposure in 0.01 M solution confirmed the presence of pitting corrosion.

The corrosion potential, E_{corr}, of 403SS in 0.1 M NaCl solutions at various pH values fell in the vicinity of –0.2 V; E_{corr} shifts only slightly in the direction of more negative values with a decrease in pH (Figure 2-2).

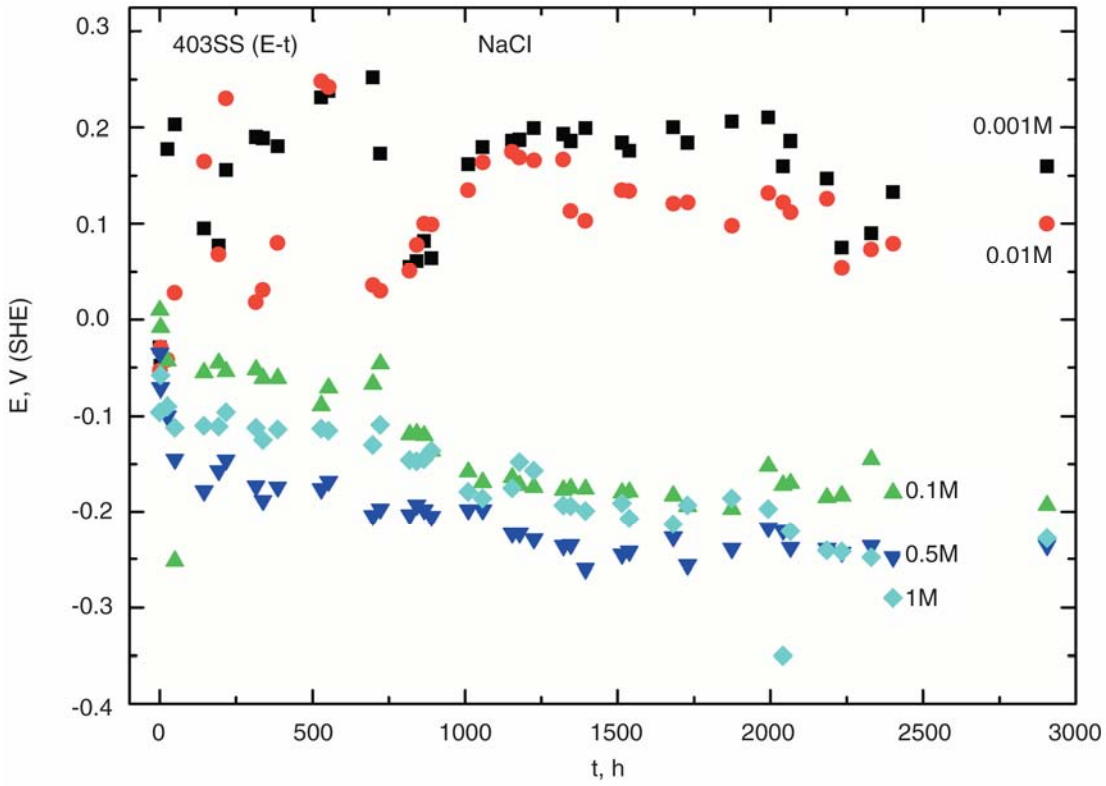

Figure 2-1
Time-variation of corrosion potential of steel 403SS in NaCl solutions of various concentrations; pH 6; temperature of 20°C (68°F).

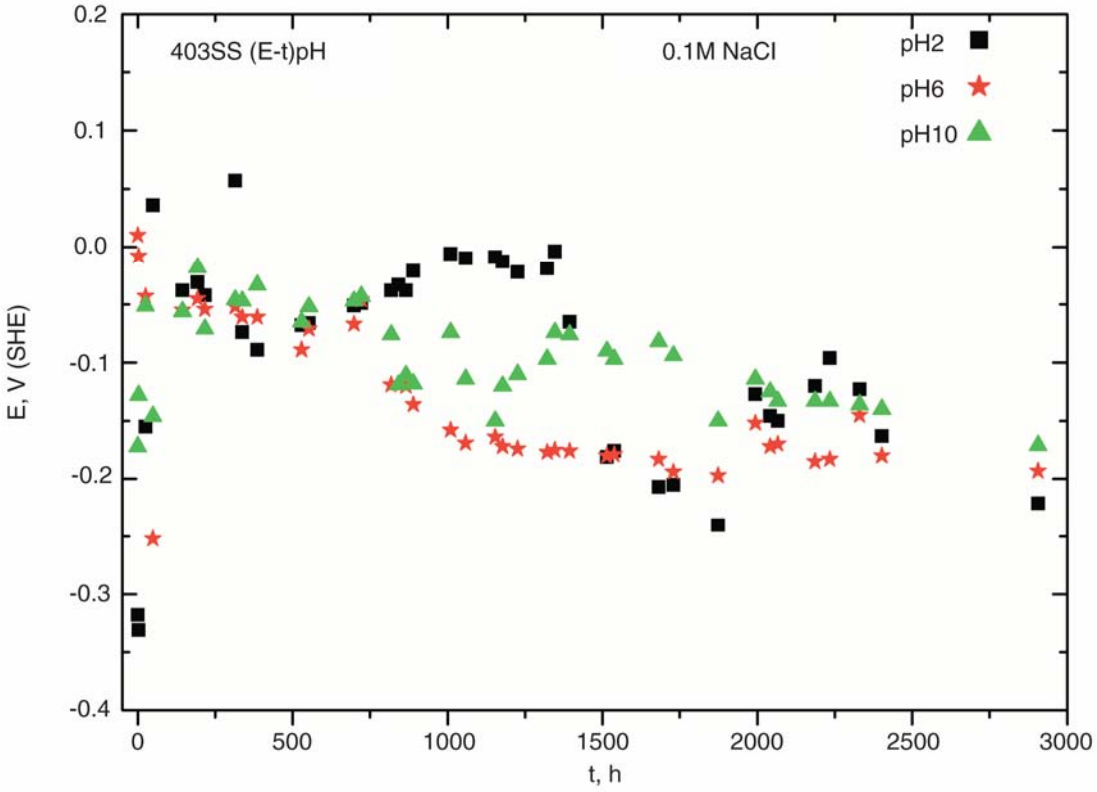

Figure 2-2
Time-variation of corrosion potential of steel 403SS in 0.1 M NaCl solutions with various pH values; temperature of 20°C (68°F).

2.1.2 Steel A470/471

Figures 2-3 and 2-4 give the results of longterm measurements of corrosion potential, E_{corr}, of A470/471 steel in the NaCl solutions of several concentrations ranging from 0.001 to 1.0 M and in 0.1 M NaCl solution at pH 2, 6, and 10. The values of E_{corr} shifted rather quickly in the direction of more negative values and, in all cases, reached a potential of about –0.4 V. As was shown by visual and microscopic analysis of the surface of test steel specimens after holding them in the NaCl solutions for various periods of time, a shift of potential in the negative direction is associated with the development of pitting. Probably, E_{corr} reaches a virtually constant value, when a sufficiently large fraction of specimen surface is activated by the aggressive chloride ion, and this value of E_{corr} corresponds to the activated surface, whereas the initial E_{corr} corresponds to the state resulting from the interaction of the metal surface with water, which, as a rule, is a passivator.

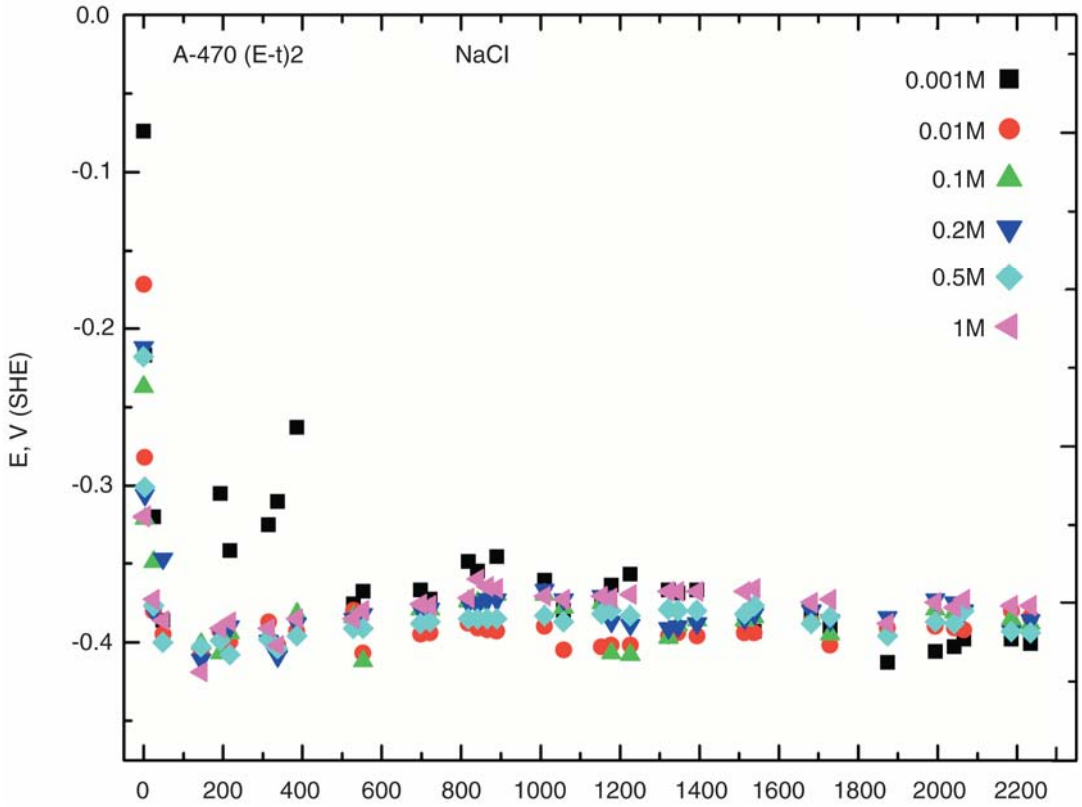

Figure 2-3
Time-variation of corrosion potential of steel A470/471 in the NaCl solutions of various concentrations; pH 6; temperature of 20°C (68°F).

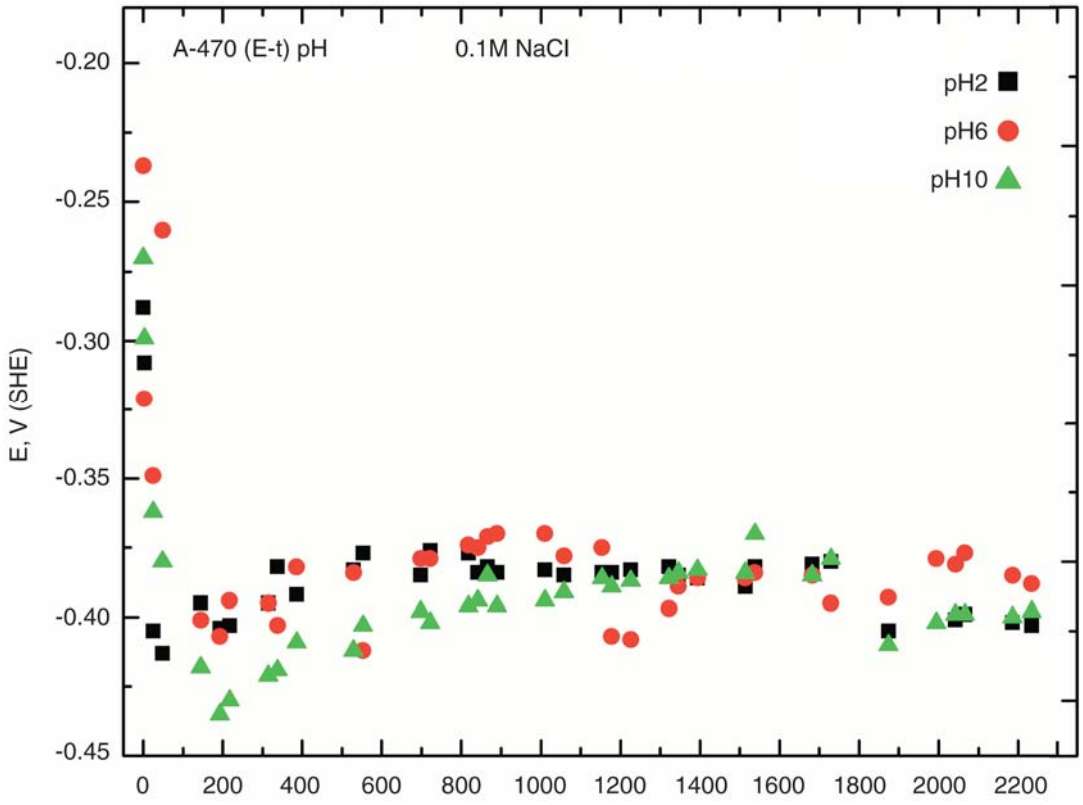

Figure 2-4
Time-variation of corrosion potential of A470/471 steel in 0.1 M NaCl solutions with various pH values; temperature of 20°C (68°F).

2.2 Cathodic Processes on Steels 403SS and A470

Two cathodic reactions that are most probable in the corrosion process of 403SS and A470/471 steel in the NaCl solutions were studied: the hydrogen evolution and the dissolved oxygen reduction. These reactions were studied in the temperature range from 20°C to 95°C (68°F to 203°F), with pH from 4 to 10 (some dependences were measured in the pH range from 2 to 10), and dissolved oxygen contents from 100% (saturation) to 1%. The studies were performed by using potentiodynamic techniques, in which the potential is swept linearly with time and the current is recorded. The results enable characterization of these two principal cathodic reactions of the corrosion process: the reduction of dissolved oxygen and hydrogen evolution. The kinetic equations of oxygen reduction relating the process rate (the current density) to the overpotential of reaction were obtained. The kinetic equations for the hydrogen evolution process according to two mechanisms—the discharge of hydroxonium ions and the discharge of water molecules—were obtained. It was shown that for pH ≤ 4, hydrogen evolution proceeds via the reduction of H^+, whereas in more basic solutions the principal reaction is the reduction of H_2O. Thus, the ranges of pH values at which hydrogen evolution proceeds by each of these mechanisms were determined.

By way of illustration, Figure 2-5 shows the dependence of the logarithm of the cathodic evolution current on the logarithm of hydrogen ion concentration in the solution at a potential of –0.67 V for A470/471 turbine rotor/disc steel. It is seen that, in the pH range from 8 to 6, the rate of cathodic evolution only slightly increases with a decrease in the solution pH. Obviously, in this pH range, the reaction proceeds predominantly via the reduction of water molecules: $2H_2O + 2e \rightarrow H_2 + 2OH^-$. Over the pH range from 5 to 2, however, the character of the dependence changes: the hydrogen evolution rate steeply increases with solution acidification. As follows from Figure 2-5, in this pH range the reaction order of hydrogen cathodic evolution with respect to hydrogen ions is 0.757, indicating that the hydrogen evolution proceeds by the mechanism $2H^+ + 2e \rightarrow H_2$.

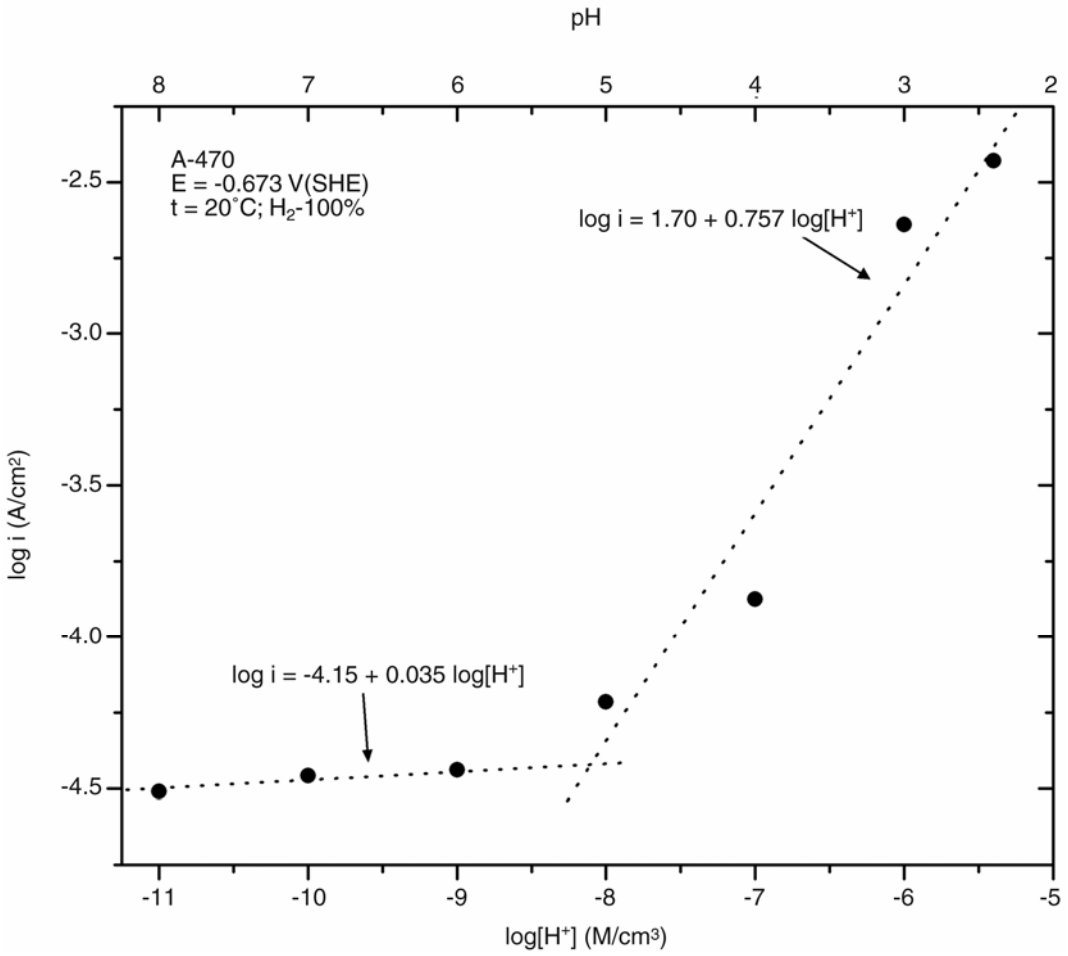

Figure 2-5
The effect of the bulk concentration of H^+ (pH) on the rate of hydrogen cathodic evolution on A470/471 steel in 0.01 M NaCl solution at 20°C (68°F) and at a potential of –0.67 V.

Figure 2-6 yields the cathodic polarization curve (the dependence of cathodic current density i on the overpotential η), which was obtained experimentally for hydrogen evolution on A470/471 in

0.01 M NaCl solution with pH = 4 at 20°C (68°F). To approximate the experimental curve, an equation describing the mixed kinetics of electrode processes was used:

$$i = - i_0 \left(1 - \frac{i}{i_d} \right)^p exp\left(- \frac{\alpha F \eta}{RT} \right)$$ **Equation 2-1**

where i_o is the exchange current density, i_d is the limiting diffusion current density, α is the transfer coefficient, F is the Faraday number, R is the gas constant, and T is the temperature. The magnitudes of the parameters providing good agreement between the experimental results (circles) and calculated data (dotted line) were determined: $i_o = 4.85 \times 10^{-6}$ A/cm^2, p = 0.757, $\alpha = 0.315$, and $i_d = 1.4 \times 10^{-4}$ A/cm^2 . Application of this equation, which accounts for the diffusion stage, incorporates both activation and diffusion in controlling the reaction rate, and appears especially appropriate when no pronounced Tafel curve region is observed in the experimental plots.

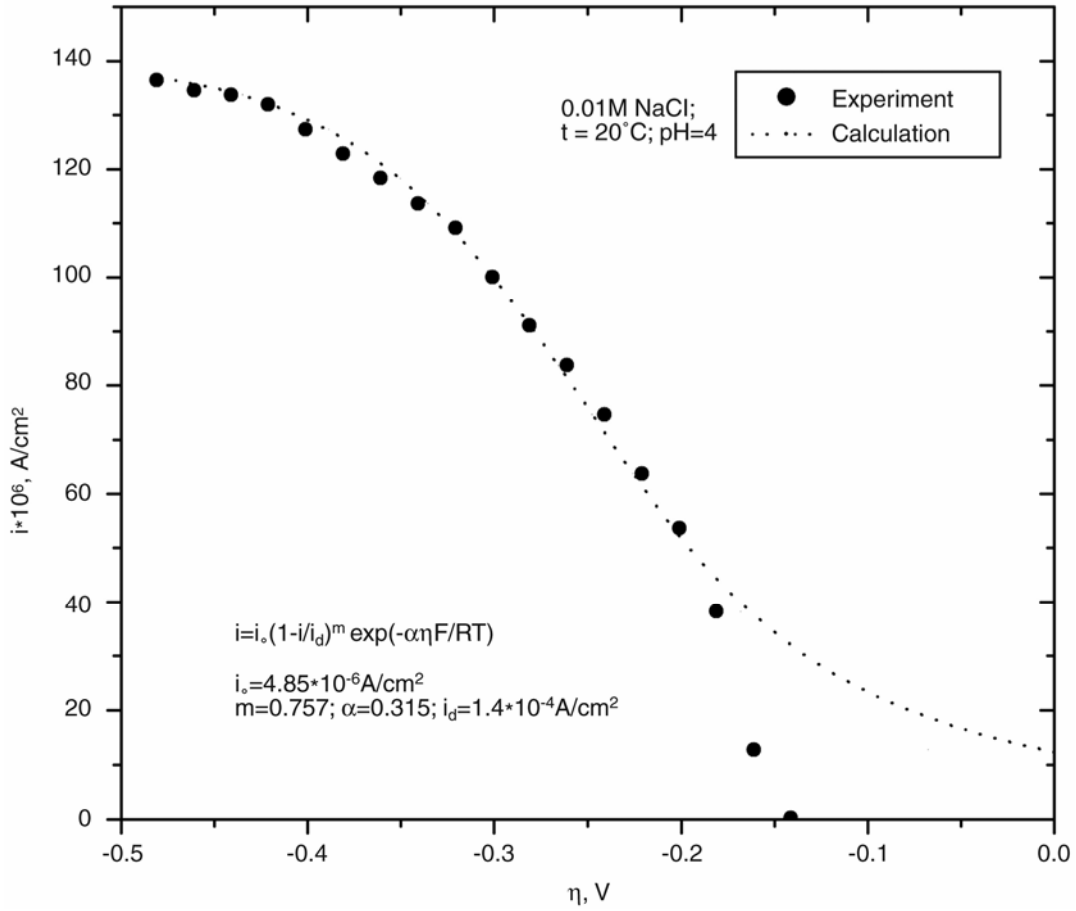

Figure 2-6
Plots of the current density of hydrogen evolution vs. overpotential based on the experimental results (circles) and calculated data (the dotted line) using Equation 2-1, taking into account the variation in the solution sH^+ concentration near the cathode.

Figure 2-7 shows a plot of limiting cathodic current density vs. the oxygen concentration in the solution for A470/471 steel. The linear character of the plot shows that oxygen diffusion controls the process rate under these conditions. Similar (linear) plots are observed at other pH values and temperatures of the solution.

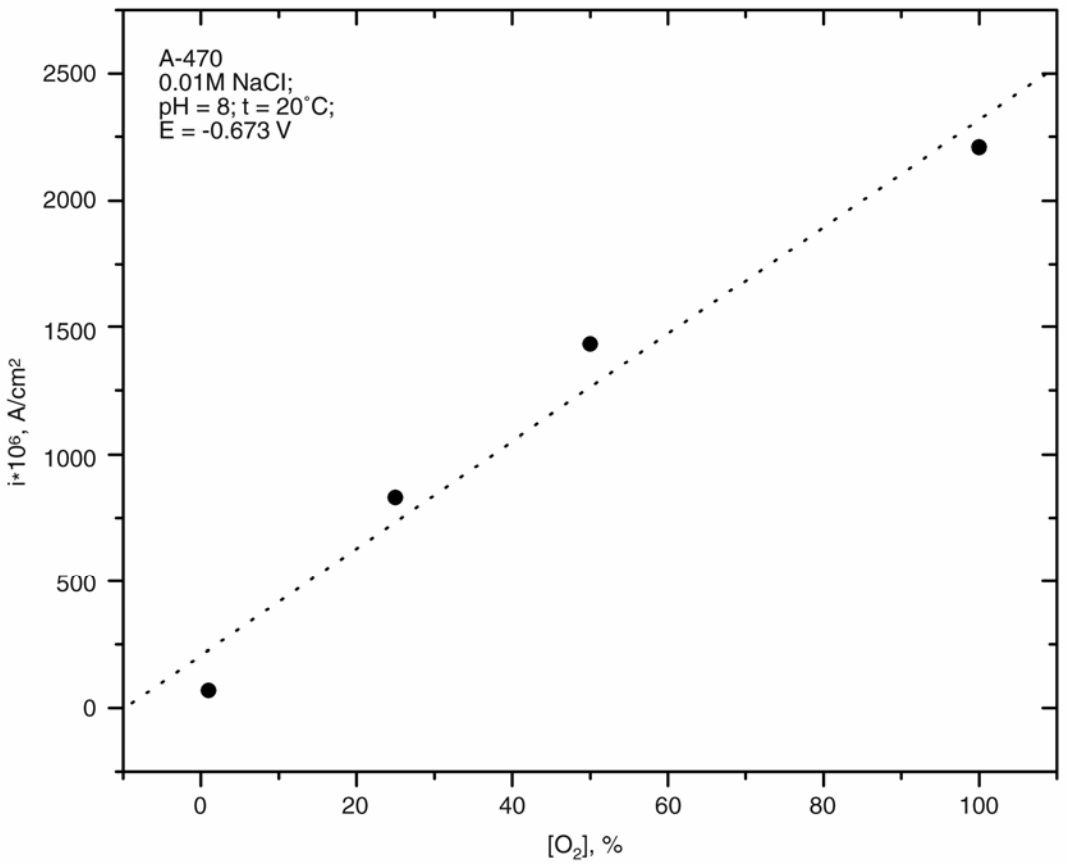

Figure 2-7
Dependence of current density for oxygen reduction on A470/471 steel at a potential of –0.663 V , temperature of 20°C (68°F), and pH 8 on the degree of oxygen saturation of the 0.01 M NaCl solution (100% saturation corresponds to an oxygen solubility of 1.36 x 10^{-6} M/cm^3).

Figure 2-8 displays the polarization curves for oxygen reduction on 403SS at various electrode rotating rates. In these curves, the limiting current range is observed; it is seen that the limiting current substantially depends on the electrode rotational rate, as expected.

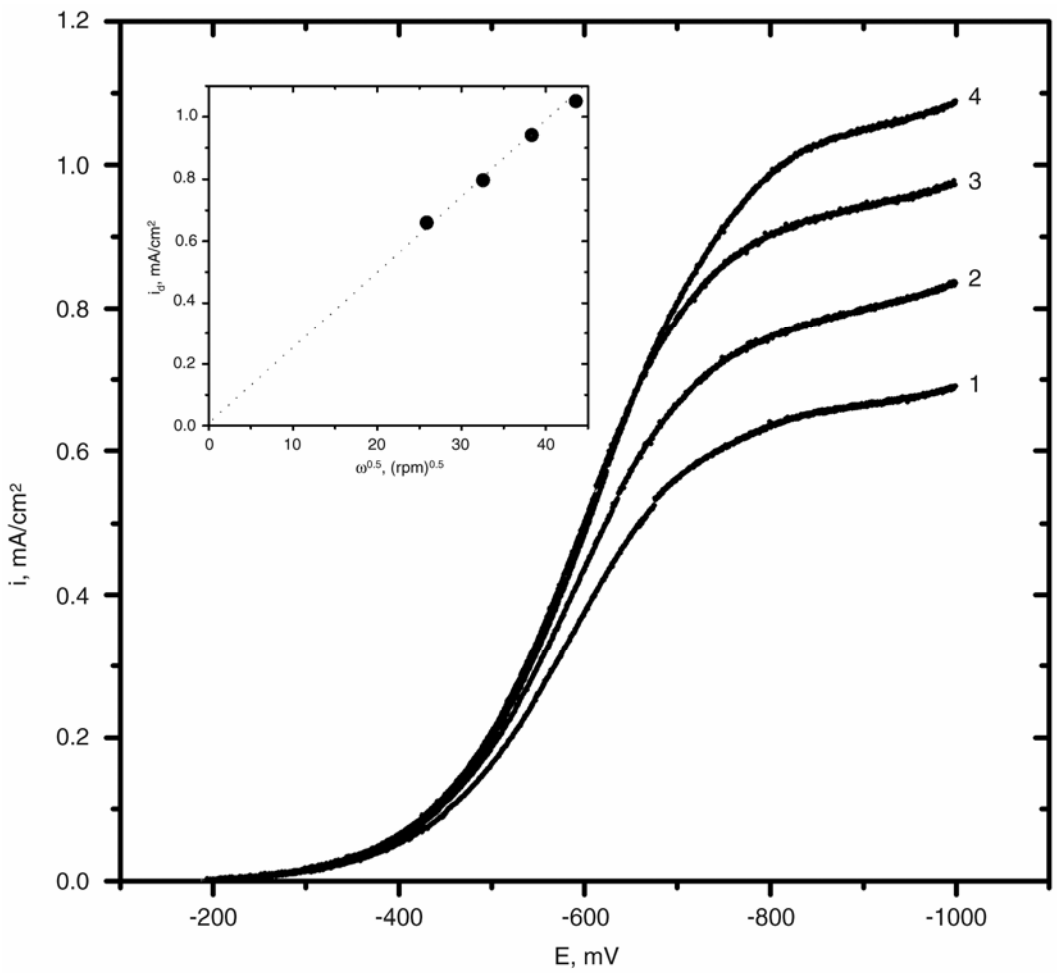

Figure 2-8
Polarization curves for oxygen electroreduction on a rotating disk electrode of 403SS at rotational rates of (1) 670 rpm, (2) 1060 rpm, (3) 1460 rpm, and (4) 1900 rpm. The inset gives the dependence of the limiting current for oxygen electroreduction on the square root of the electrode rotational rate (the experimental data [circles] and calculated data [dotted line]); a linear relationship is predicted by the Levich equation.

On iron and steels of various compositions, in some cases the limiting current is observed in the potential range where the electroreduction of oxygen takes place. The current is limited by diffusion and, in the experiments with the rotating disk electrode, obeys the Levich equation [10]. In other cases, the dependence of the oxygen reduction current on the rate of oxygen delivery to the electrode surface is not pronounced, and its character depends on the time of electrode exposure to the electrolyte solution or on the pretreatment of the electrode surface [8-10]. This is caused by the dependence of the oxygen reduction rate on the properties of the surface oxide layer, which are determined by various factors.

When the limiting current is controlled by diffusion, in accordance with the Levich equation [10], i_d is linearly proportional to the square root of the electrode rotational rate, ω:

$$i_d = 0.62\, nFc_oD^{2/3}\nu^{1/6}\omega^{1/2} \qquad \textbf{Equation 2-2}$$

where n is the number of electrons involved in the reaction; c_o is the bulk concentration of reagent; D is the diffusion coefficient; ν is the solution viscosity; and ω is the electrode rotational rate. In the calculations reported here for the rate of oxygen electroreduction, the following magnitudes of these parameter values were used: n = 4; $c_o = 2\ 10^{-7}$ M/см^3; $D = 2\ 10^{-5}$ см^2/ с; and $\nu = 10^{-2}$ см^2/ с . The inset of Figure 2-8 yields the dependence of the limiting current of oxygen electroreduction (from the data in Figure 2-8 at a potential of -0.75 V) on the square root of the electrode rotational rate. The dotted straight line is calculated using the Levich equation. The agreement between the experimental and calculated dependences of the limiting current on the electrode rotational rate indicates that the process is controlled by oxygen transfer from the bulk solution to the electrode surface. The process involves four electrons; oxygen is reduced completely to water, without the accumulation of hydrogen peroxide in the near-electrode space during the course of reaction.

2.3 Determination of Corrosion Potential and Corrosion Current

To determine the corrosion rate, it is insufficient to measure only the corrosion potential, because the rate of the anodic oxidation of the steel substrate and its dependence on potential and other independent parameters must be also known. Moreover, the direct method of measuring E_{corr}, which was used in the previous section, is very time consuming.

To predict the damage accumulated by uniform corrosion, the principle of charge conservation is commonly used [12]. At the corrosion potential (it is assumed to be identical over the entire specimen surface and constant in time), the current densities of cathodic and anodic reactions are equal. Commonly, the Tafel portions of anodic (metal dissolution) and cathodic (reduction of dissolved oxygen in neutral aqueous salt solutions) polarization curves are measured experimentally and extended until they intersect each other. The corrosion potential and the corresponding corrosion current are determined by the intersection point, and the corrosion current is converted into the linear or weight corrosion rate. According to the same principle, in the case of pitting corrosion, E_{corr} can be determined by the coordinate of the intersection of the extended cathodic Tafel portion and extended anodic polarization curve corresponding to the passive metal state, because pits form on the passive surface. Therefore, it is assumed that pitting does not change the specimen potential, because the fraction of surface occupied with pits is small. In some cases, this is indeed so [13]; in this work it was found that E_{corr} varies with time in the chloride solutions employed.

In order to determine the dissolution rate (the dissolution current density) of the metal in a pit at the corrosion potential, it is necessary to obtain the anodic polarization curve corresponding to the metal dissolution in a pit, and to then extrapolate the curve to the corrosion potential. These curves were obtained according to the procedure described earlier (by the reverse potentiodynamic anodic curve after total activation of the entire surface of the test specimen).

The cathodic polarization curves were obtained by extending the reverse anodic potentiodynamic curve to the range of cathodic potentials. In the anodic and cathodic polarization curves, the Tafel portions were found; then, by their intersection, E_{corr} was determined, which corresponds to the stage of developed pitting corrosion—that is, the stage when the potential is determined by the potential of steel surface activated by chloride ions, but not by the potential of passive surface. These experiments were performed at several concentrations of NaCl in the solution, and at several pH values and temperatures of 0.1 M NaCl solution. By way of illustration, Figure 2-9 shows the anodic and cathodic polarization curves plotted on the semilogarithmic coordinates, which were obtained for steel 403SS in 1 M NaCl solution with pH = 6 at 20°C. The intersection point of the anodic and cathodic Tafel portions yields E_{corr} = −0.24 V. (This value is close to the corrosion potential, which is reached in the long-term measurements of E_{corr} and corresponds to highly developed pitting; see Figure 2-1.) The current density of metal dissolution in the pits at this potential is 3.5 x 10^{-6} A/cm^2.

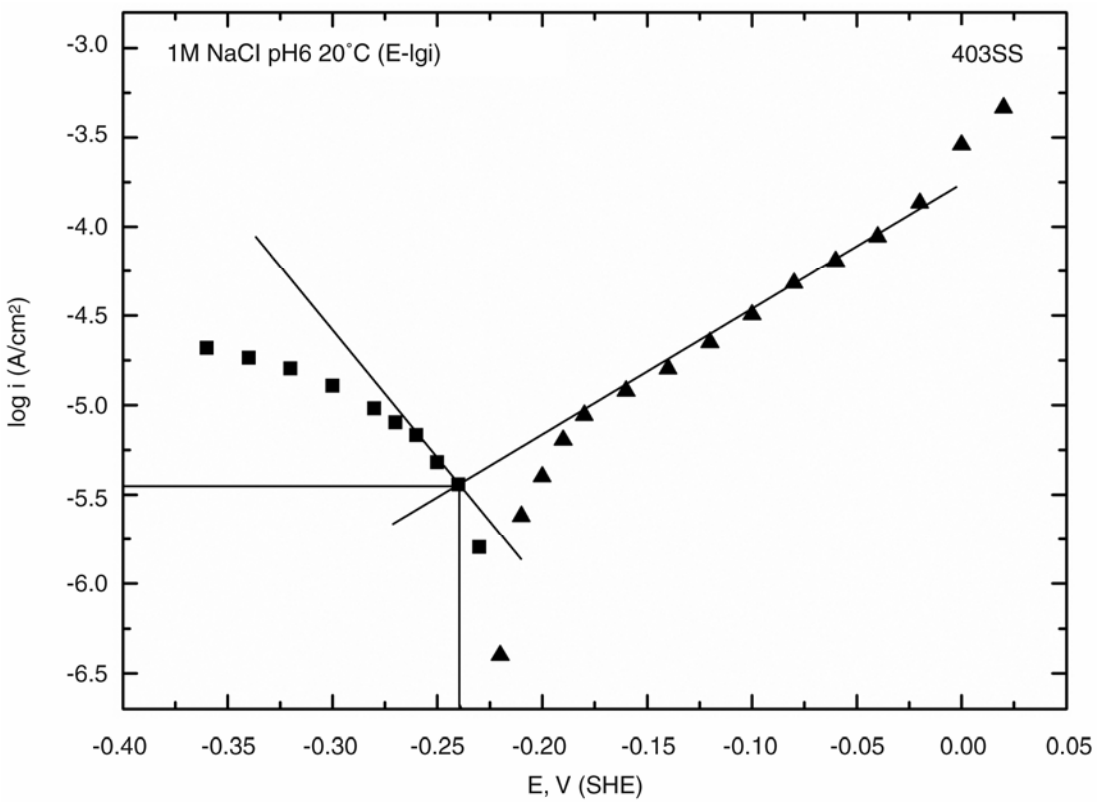

Figure 2-9
Anodic (triangles) and cathodic (squares) polarization curves of 403SS in 1 M NaCl solution with pH = 6 at 20°C (68°F). The Tafel portions of these curves are shown with straight lines. The corrosion current and corrosion potential are determined by the coordinates of the intersection of the straight lines.

The current density of metal dissolution in a pit at the initial stage of the corrosion process can be determined as the current density in the anodic polarization curve corresponding to the dissolution in a pit at the corrosion potential, which is observed within several minutes after dipping the test specimen into the solution (about 0 V). Under these conditions, the current

density of steel dissolution is approximately 2 x 10^{-4} A/cm^2. Thus, the rate of steel pitting dissolution decreases with time as E_{corr} shifts in the direction of more negative values.

The corrosion potentials and corrosion currents in the pits were determined by the above method in NaCl solutions with concentrations of 0.1 to 1.0 M (at lower concentrations, the experiments failed to achieve the total activation of the entire electrode surface in order to obtain the anodic polarization curve corresponding to steel dissolution in a pit), in 0.1 M NaCl solution with pH = 2, 6, and 10, and in 0.1 M solution with pH = 6 at temperatures of 20°C, 50°C, and 85°C (68°F, 122°F, and 185°F). Figures 2-10 to 2-17 give the results for 403SS.

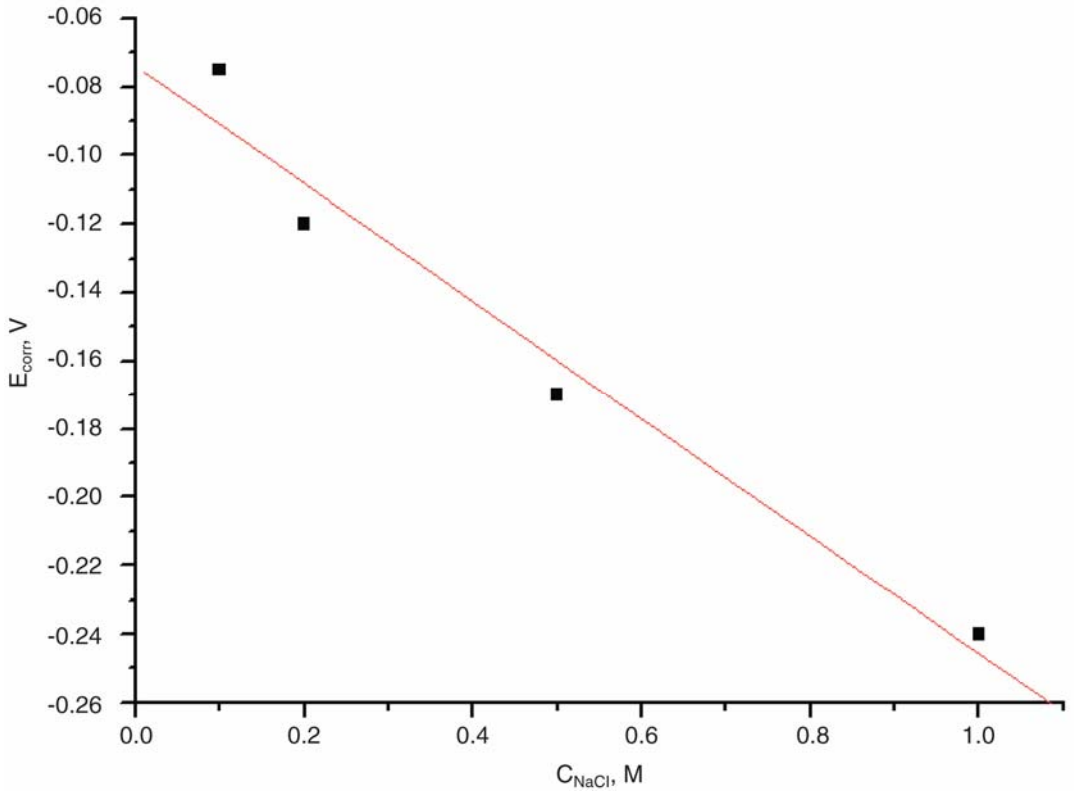

Figure 2-10
Corrosion potential of steel 403SS vs. the concentration of NaCl in solutions with pH = 6 at 20°C (68°F).

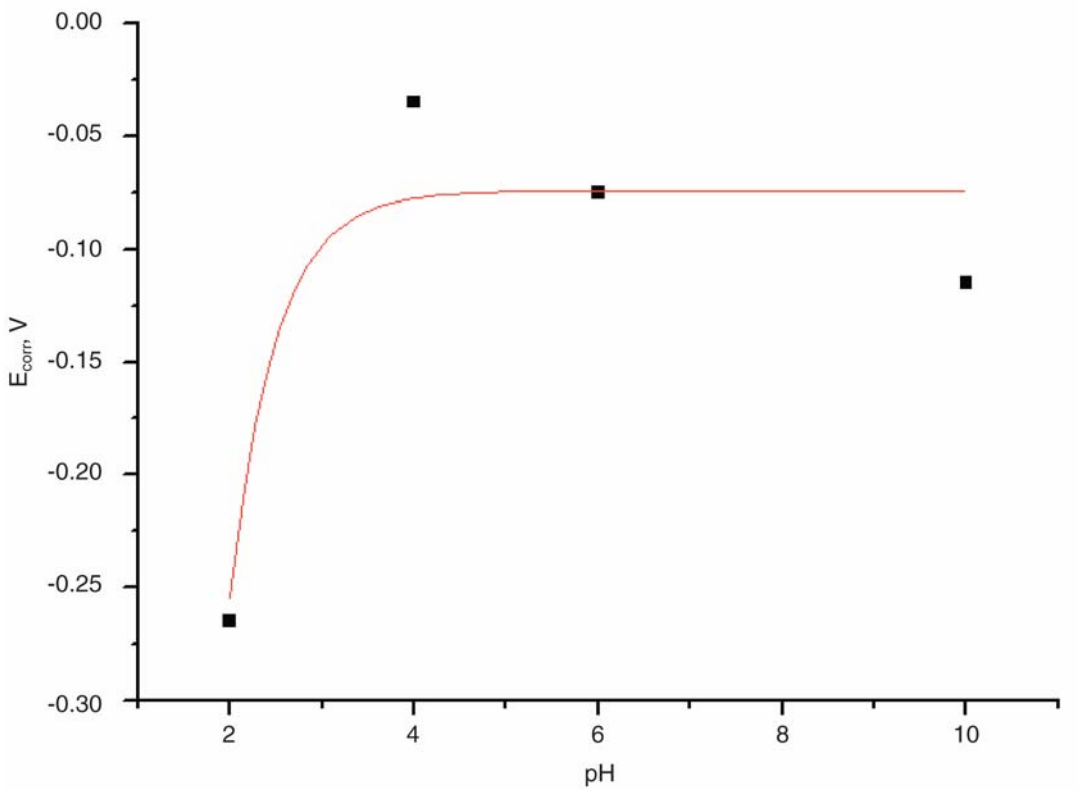

Figure 2-11
Corrosion potential of 403SS vs. pH value in 0.1 M NaCl solution at 20°C (68°F).

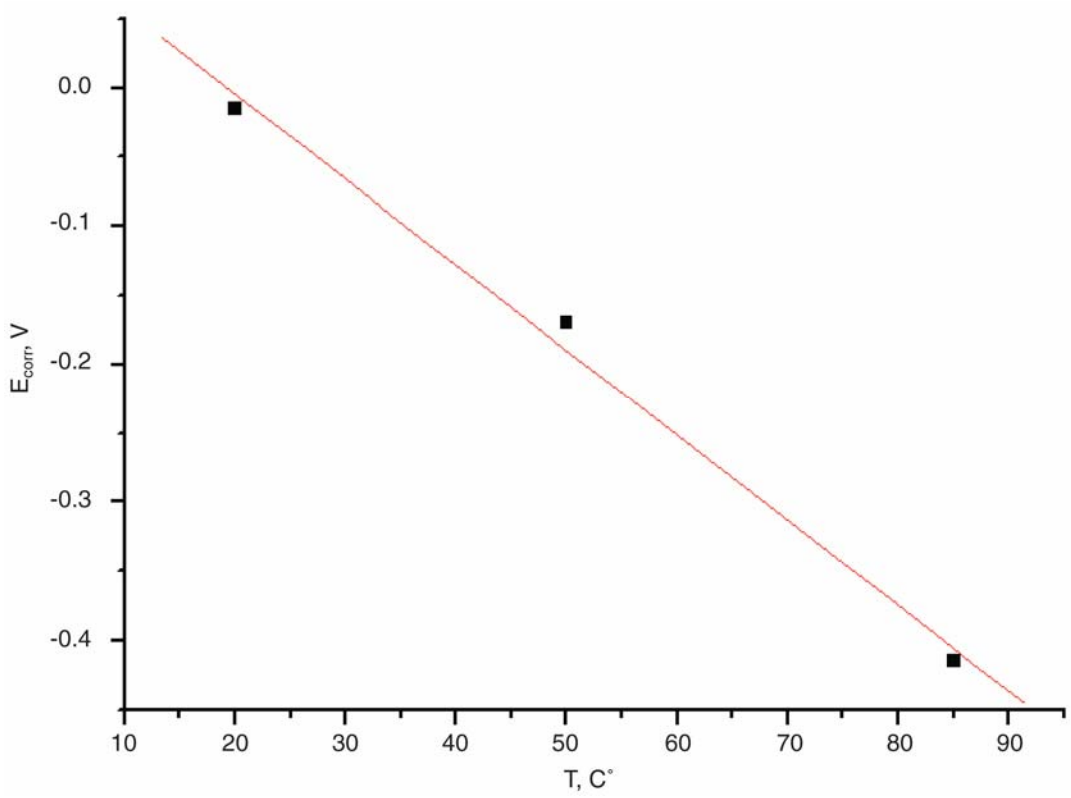

Figure 2-12
Corrosion potential of steel 403SS vs. temperature in 0.1 M NaCl solution with pH = 6.

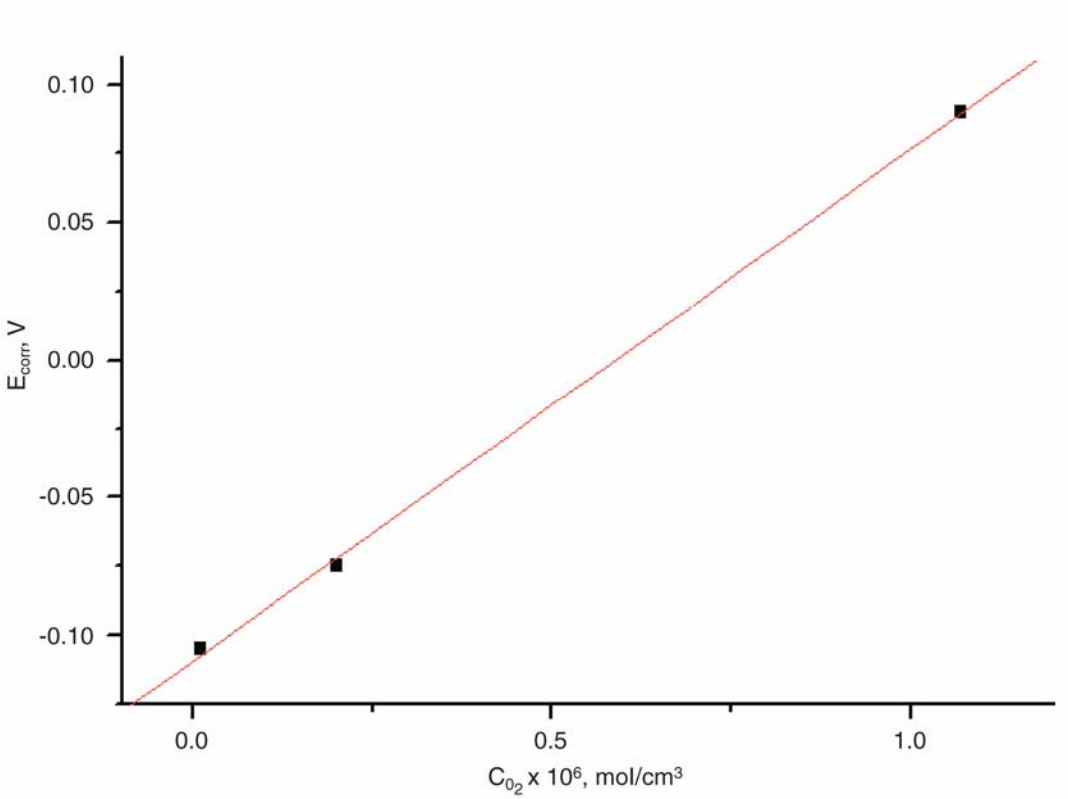

Figure 2-13
Corrosion potential of steel 403SS vs. oxygen concentration in 0.1 M NaCl solution with pH = 6 at 20°C (68°F).

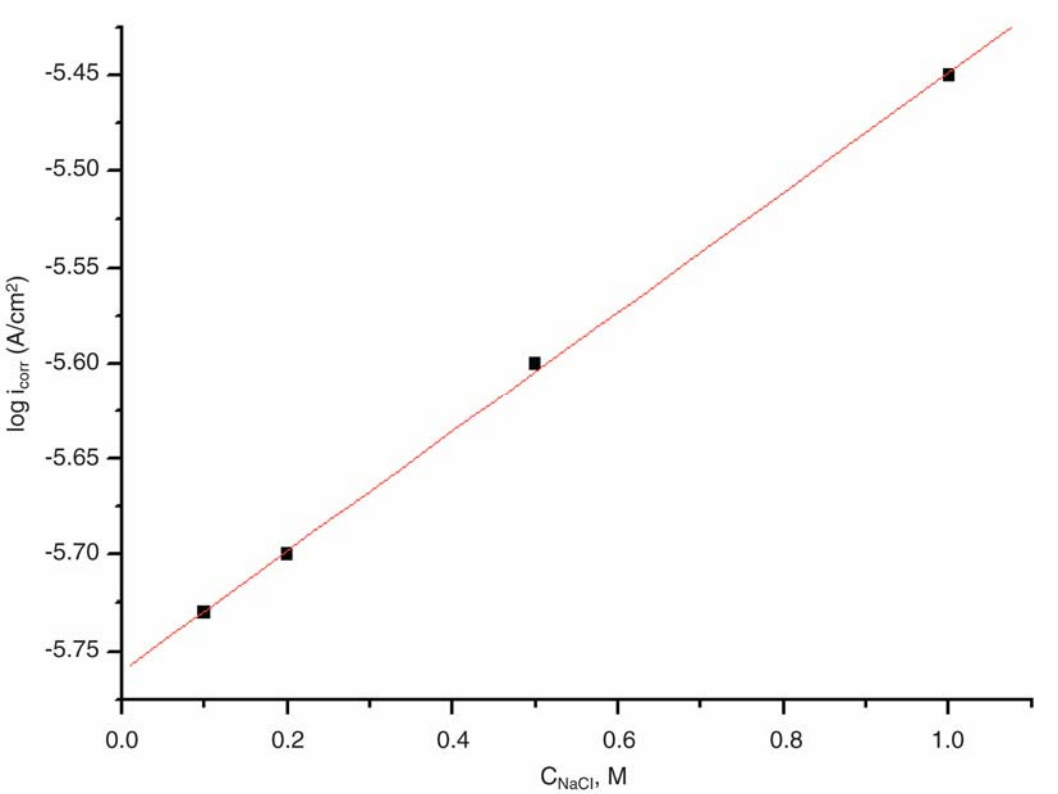

Figure 2-14
Corrosion current in the pits on 403SS vs. concentration of NaCl with pH = 6 at 20°C (68°F).

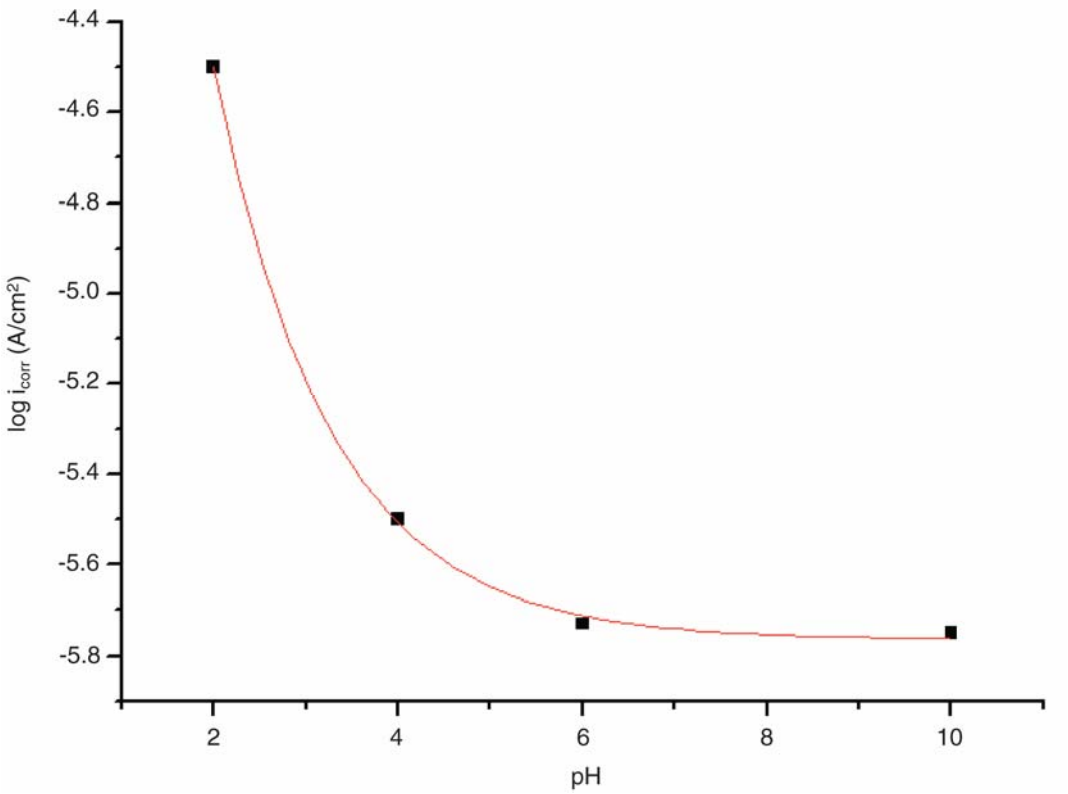

Figure 2-15
Corrosion current in the pits on 403SS vs. pH of 0.1 M NaCl solution at 20°C (68°F).

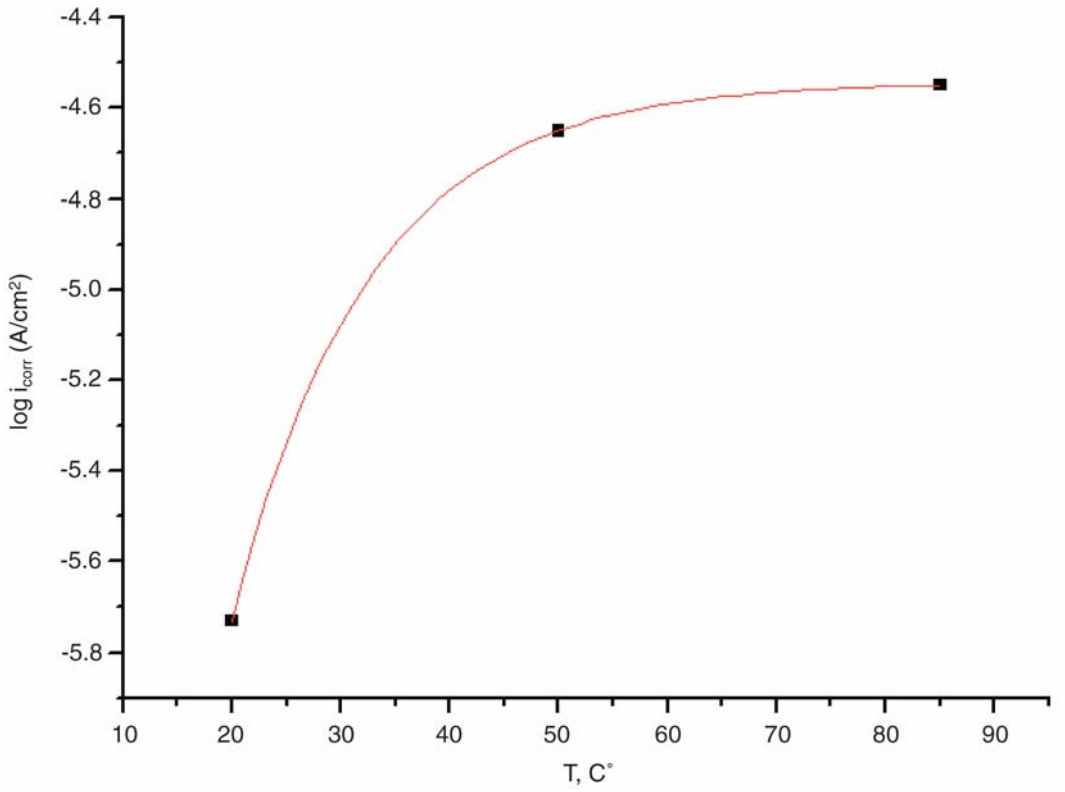

Figure 2-16
Corrosion current in the pits on 403SS vs. temperature in 0.1 M NaCl solution with pH = 6.

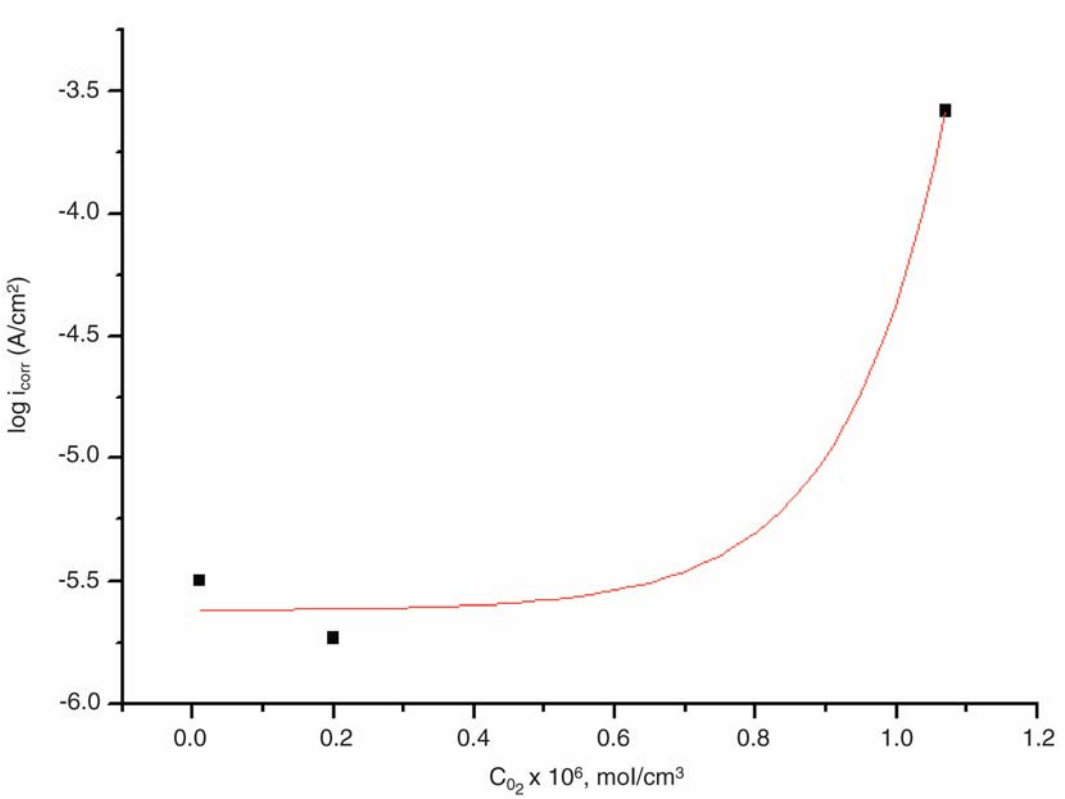

Figure 2-17
Plot of corrosion current in the pits on 403SS vs. oxygen concentration in 0.1 M NaCl solution with pH = 6 at 20°C (68°F).

These dependences can be expressed by the following equations for the corrosion potential and the corrosion current density in the pits:

$$E_{corr} = 0.029 - 0.17 \times C_{NaCl} - 0.0062 \times T + 1.86 \times 10^{5} \times C_{O_2} - 10.4 \times \exp(-2.03pH)$$

Equation 2-3

and

$$\log(i_{corr}) = -4.63 + 0.31 \times C_{NaCl} \exp(-0.79pH) - 5.92\exp(-0.08T) + 0.0013\exp(6.86 \times 10^{6} \times C_{O_2})$$

Equation 2-4

Here, as well as in other sections of report, the potential is measured in volts against SHE; the current density is given in units of A/cm^2; the temperature is in °C; the concentration of NaCl solution is in mol/l (M); and the concentration of dissolved oxygen is in mol/cm^3.

To obtain a general equation for the corrosion potential and logarithm of the corrosion current density, the sum of the partial dependences of these dependent variables on temperature, pH, and NaCl and O_2 concentrations was approximated by linear or exponential functions, and a certain

constant was added, so that the dependence best matched the experimental data. The linear plots in Figures 2-10 to 2-17 are described by Equations 2-3 and 2-4.

The corrosion potential and corrosion current in the case of A470/471 steel were determined in the same manner as in the case of 403SS. By way of example, Figures 2-18 and 2-19 give the anodic and cathodic polarization curves in semilogarithmic coordinates, which were measured in 0.1 M NaCl solution with pH = 10 and in 1.0 M NaCl solution with pH = 6 at 20°C (68°F). On these figures, the determination of E_{corr} and i_{corr} is shown.

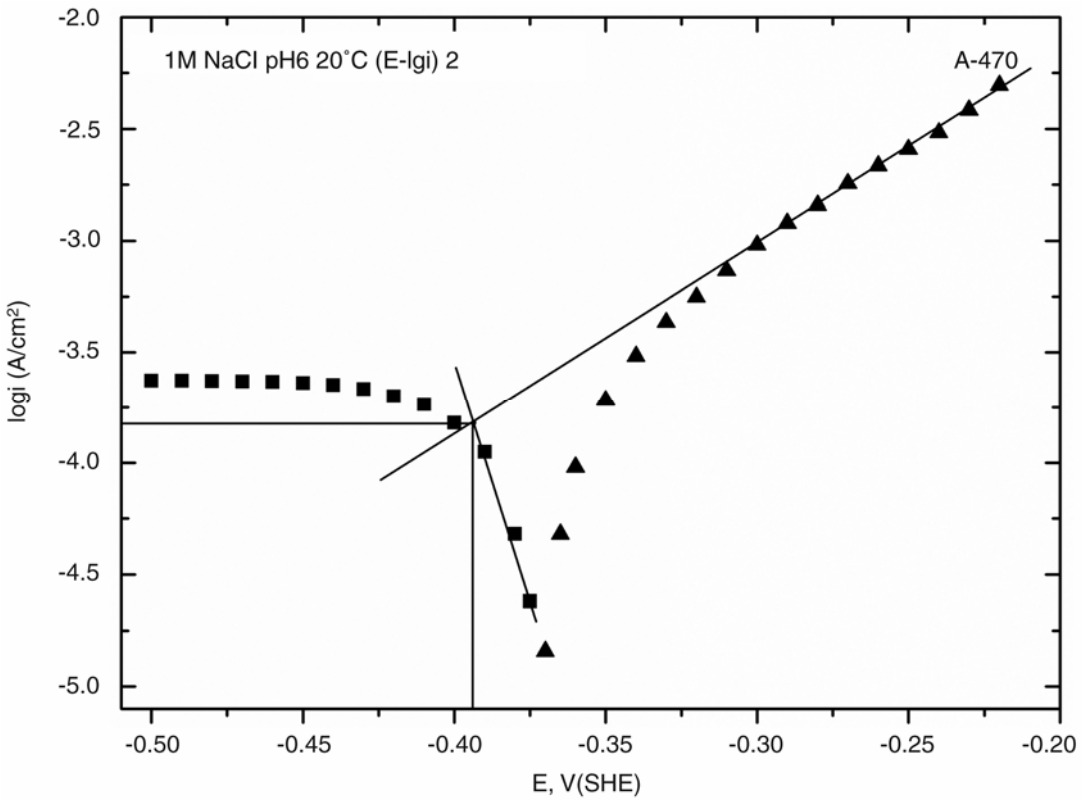

Figure 2-18
Anodic (triangles) and cathodic (squares) polarization curves for A470/471 steel in 1 M NaCl solution with pH = 6 at 20°C (68°F). The Tafel regions are shown as straight lines. The corrosion current and corrosion potential are determined by the coordinates of the intersection of the straight lines.

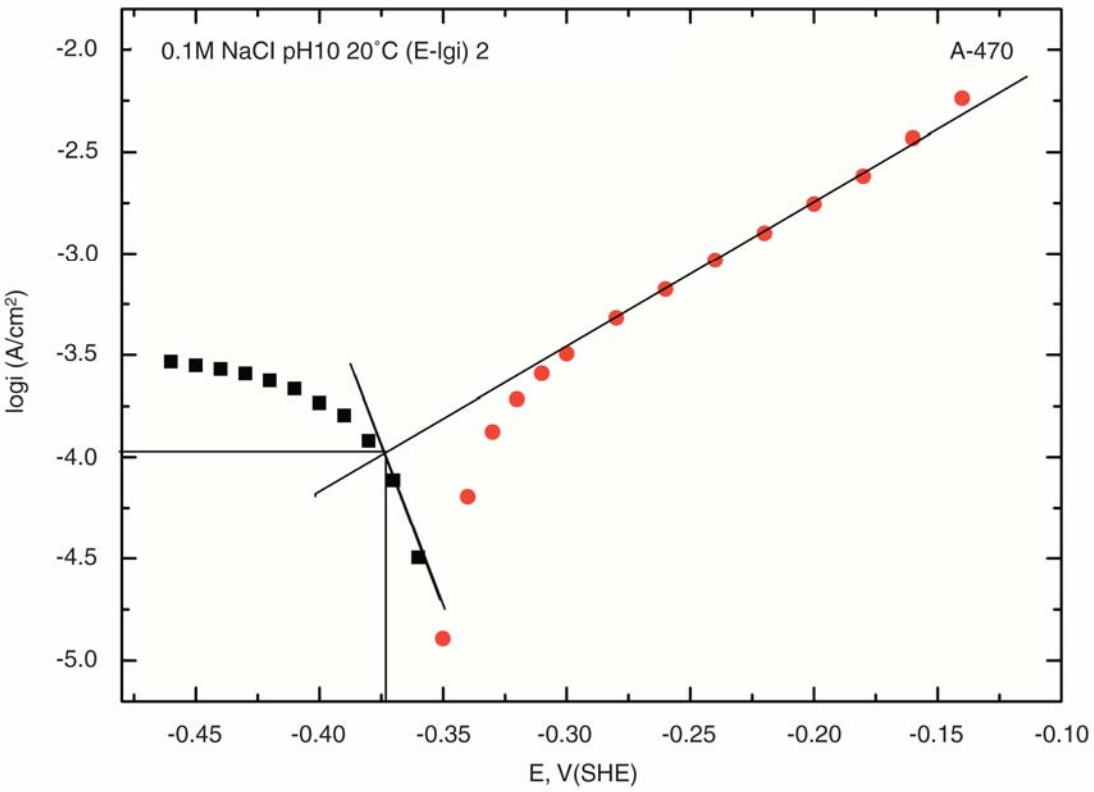

Figure 2-19
Anodic (circles) and cathodic (squares) polarization curves for A470/471 steel in 1 M NaCl solution with pH = 10 at 20°C (68°F). The Tafel regions are shown as straight lines. The corrosion current and corrosion potential are determined by the coordinates of the intersection of the straight lines.

The corrosion potential and corrosion current density in the pits were determined in the NaCl solutions with concentrations of 0.1 to 1.0 M, in 0.1 M NaCl solution with pH = 2, 6, and 10, and in 0.1 M solution of pH = 6 at temperatures of 20°C, 50°C, and 85°C (68°F, 122°F, and 185°F). Figures 2-20 to 2-27 give the results.

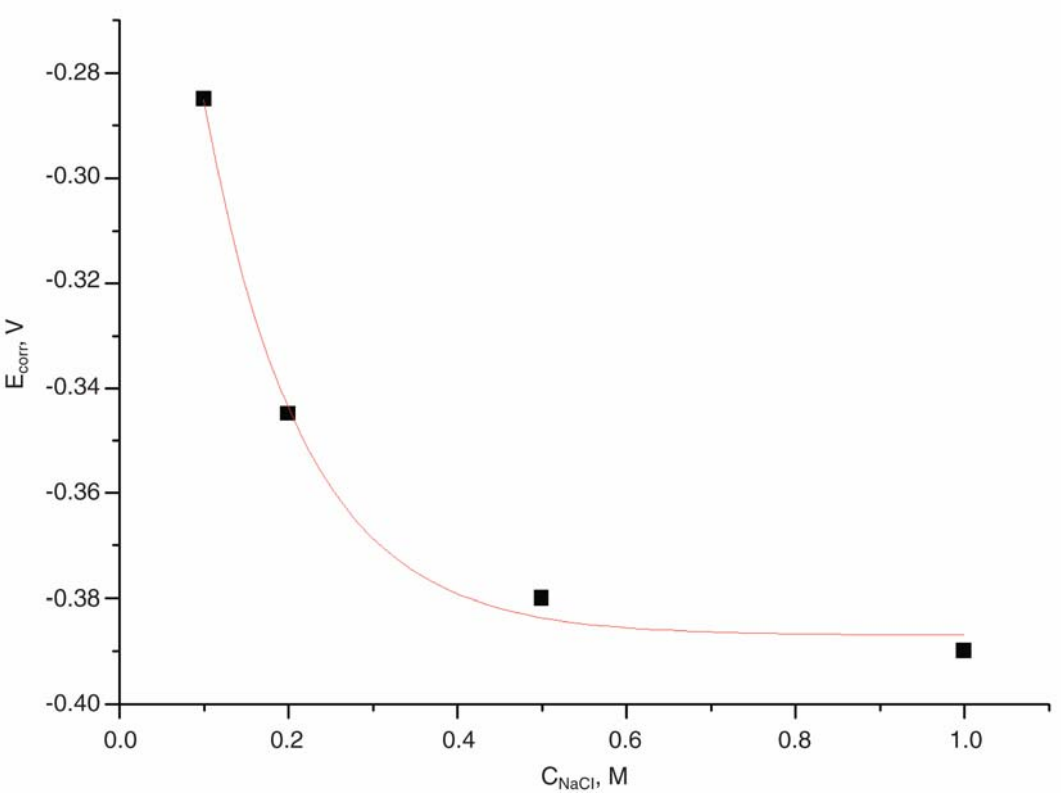

Figure 2-20
Corrosion potential of A470/471 steel vs. NaCl concentration with pH = 6 at 20°C (68°F).

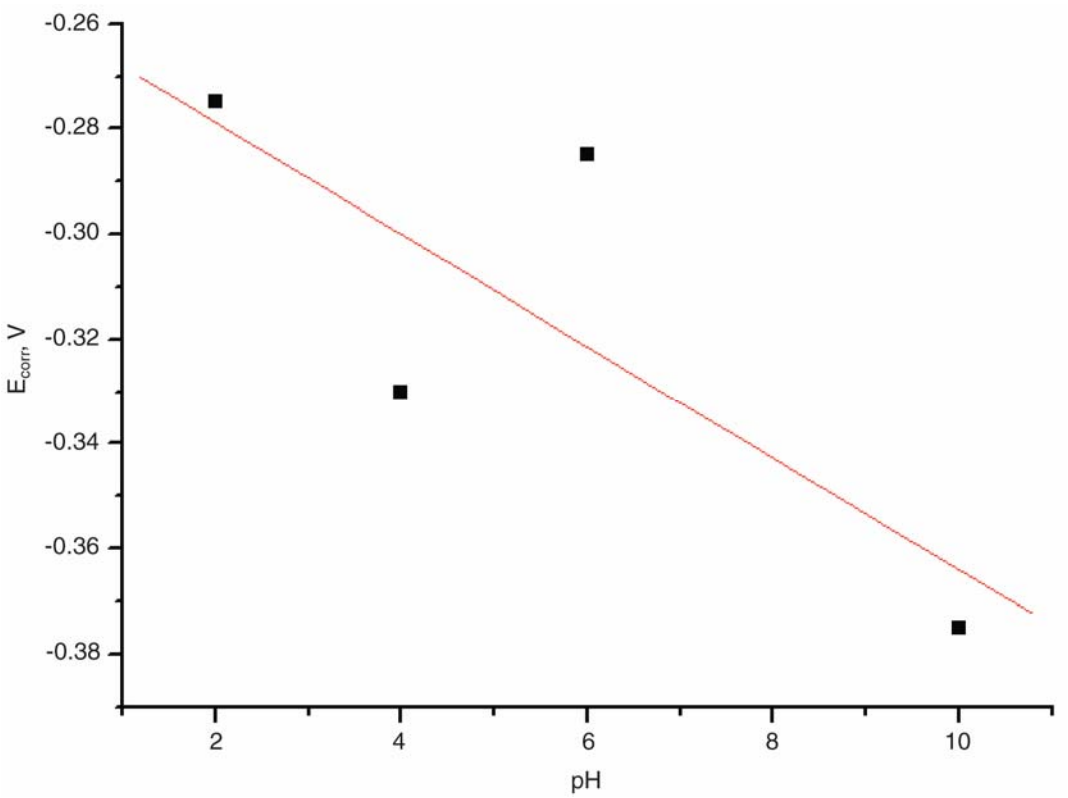

Figure 2-21
Corrosion potential of A470/471 steel vs. pH in 0.1 M NaCl solution at 20°C (68°F).

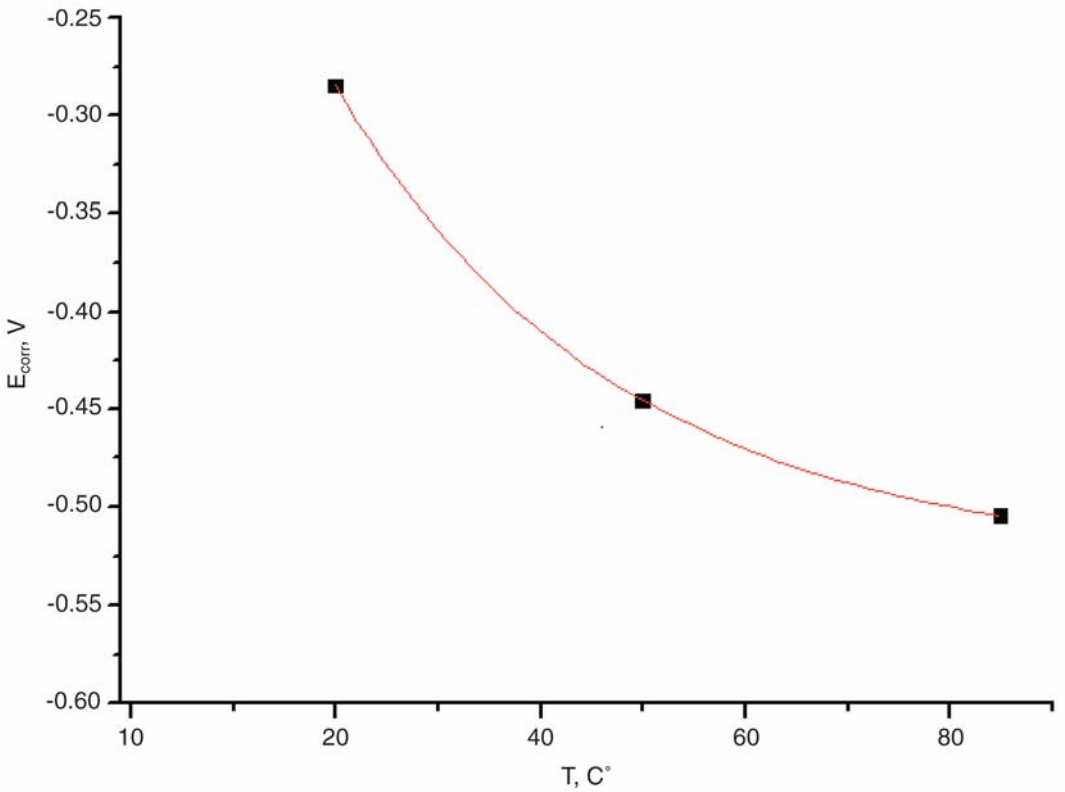

Figure 2-22
Corrosion potential of A470/471 steel vs. temperature in 0.1 M NaCl solution with pH = 6.

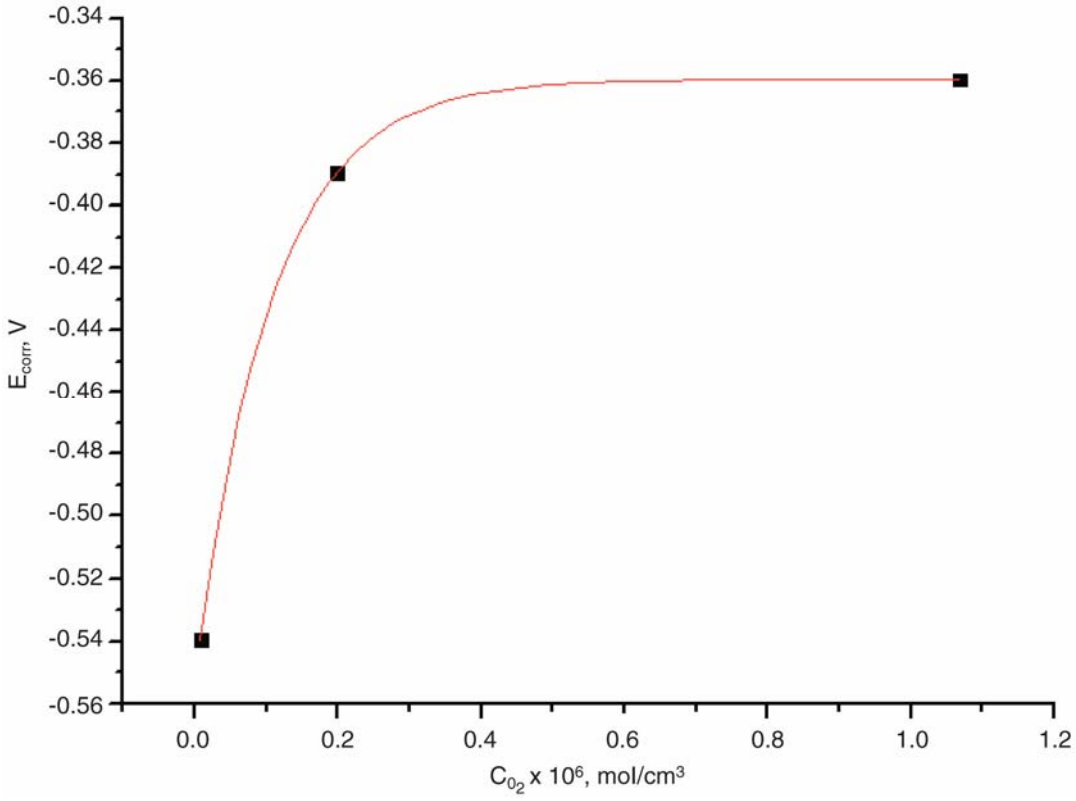

Figure 2-23
Corrosion potential of A470/471 steel vs. dissolved oxygen concentration in 0.1 M NaCl solution with pH = 6 at 20°C (68°F).

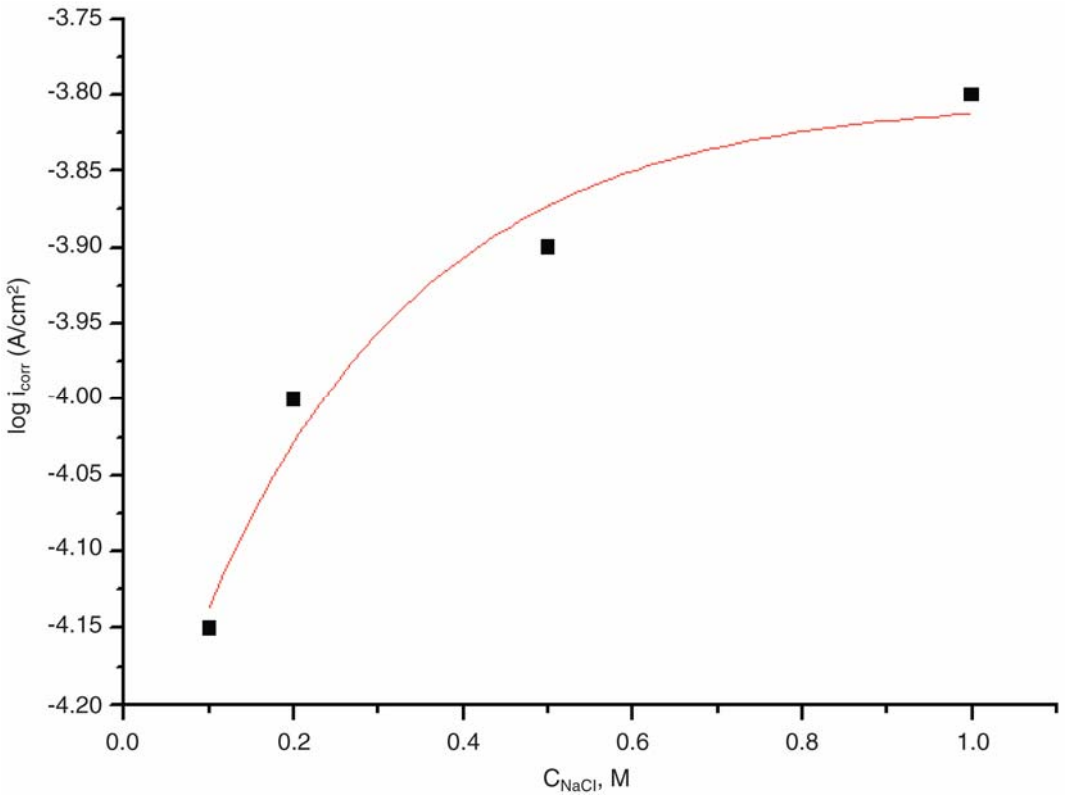

Figure 2-24
Corrosion current density for A470/471 steel vs. the concentration of NaCl in solutions with pH = 6 at 20°C (68°F).

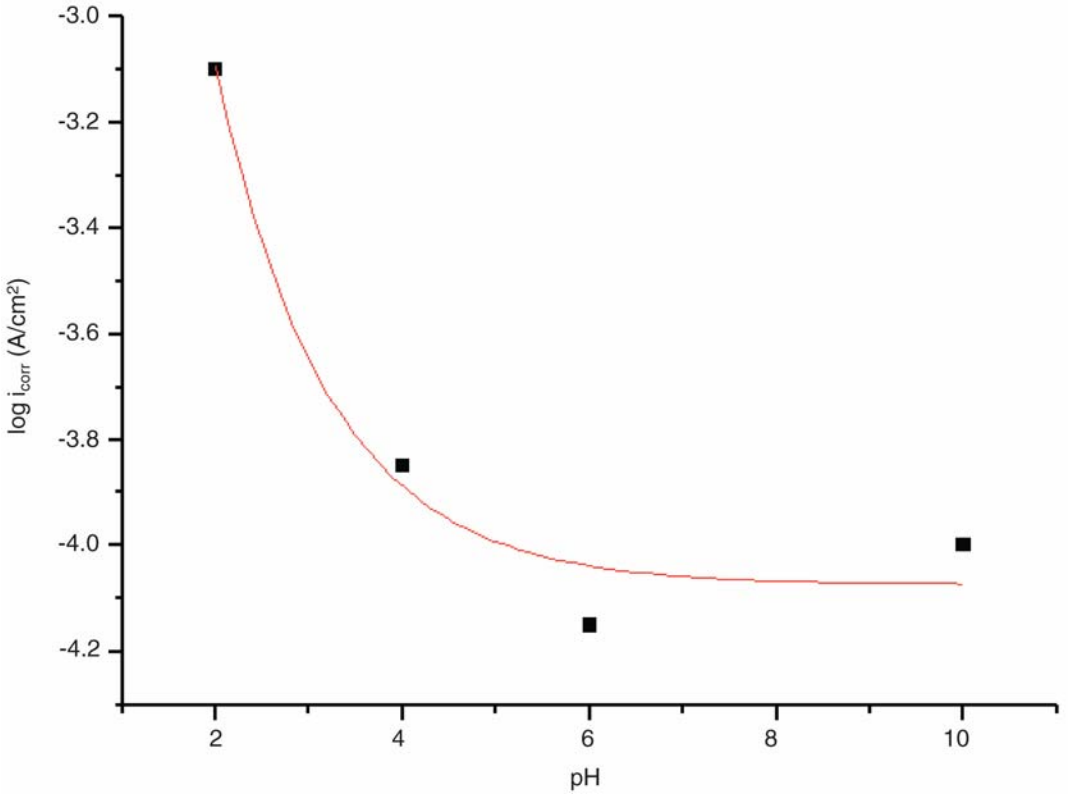

Figure 2-25
Corrosion current density for A470/471 steel vs. pH in 0.1 M NaCl solution at 20°C (68°F).

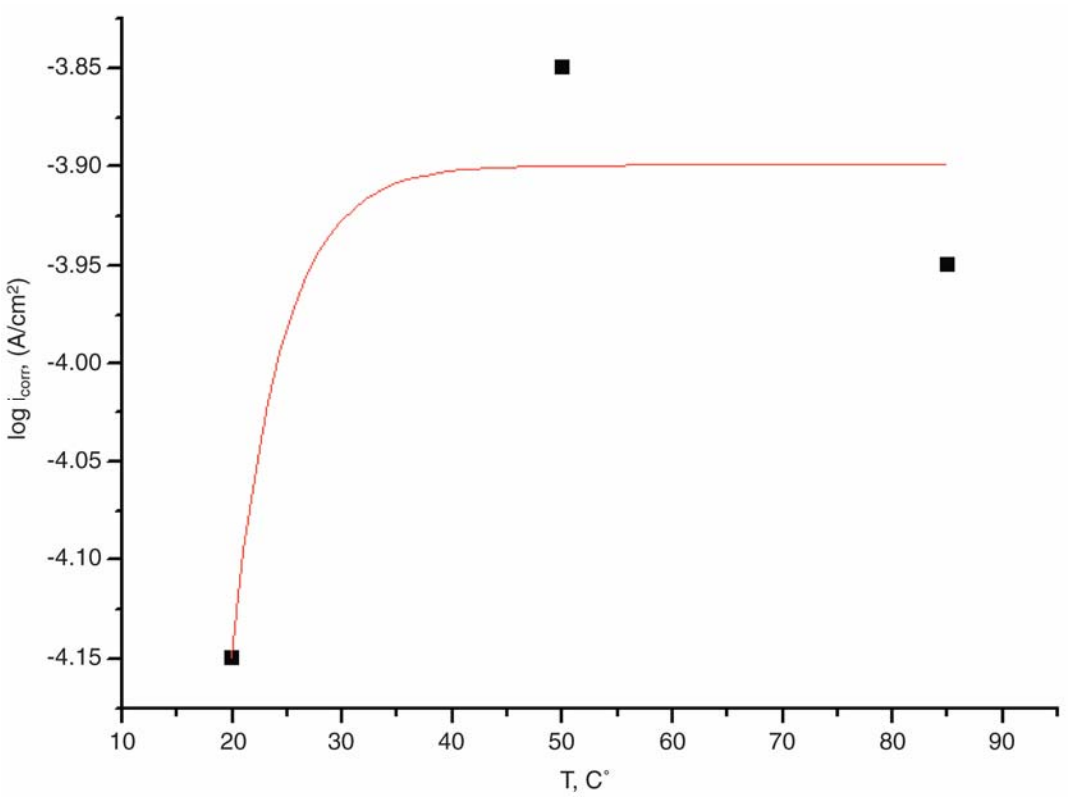

Figure 2-26
Corrosion current density for A470/471 steel vs. temperature in 0.1 M NaCl solution with pH = 6.

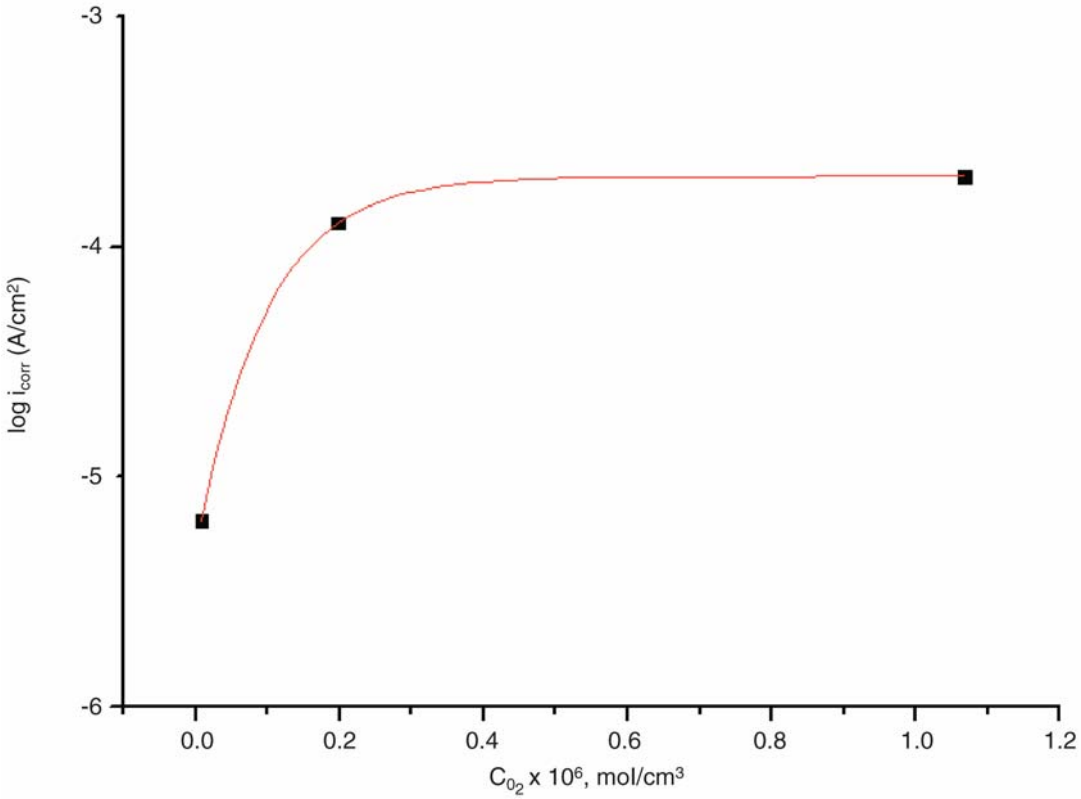

Figure 2-27
Corrosion current density for A470/471 steel vs. dissolved oxygen concentration in 0.1 M NaCl solution with pH = 6 at 20°C (68°F).

These dependences can be expressed by the following equations for the corrosion potential and the corrosion current density in the pits:

$$E_{corr} = -0.52 + 0.50\exp(-0.036 \times T) - 0.2\exp(-9.43 \times 10^{6} C_{O_2}) + 0.2\exp(-8.55 C_{NaCl}) - 0.010pH$$

Equation 2-5

and

$$\log(i_{corr}) = -3.42 - 0.49\exp(-3.88 C_{NaCl}) + 5.16\exp(-0.83pH) - 20.3\exp(-0.22 \times T) - 1.66\exp(-1.06 \times 10^{6} C_{O_2})$$

Equation 2-6

The linear plots shown in Figures 2-20 to 2-27 are described by Equations 2-5 and 2-6.

Comparing the data presented in Figures 2-1 and 2-2 with the data presented in Figures 2-10 and 2-20, it can be seen that some results obtained by different methods are not in agreement. This is primarily true for the E_{corr} values. In order to obtain quantitative data, in the above equations the results were derived from the anodic and cathodic voltammograms (examples are given in

Figures 2-9, 2-18 and 2-19). The results of longterm measurements of E_{corr} were used to demonstrate a very important effect: a pronounced change of E_{corr} with time as pitting corrosion develops. New problems arising during the experimental investigation, obviously, require further study in order to obtain more precise parameter values that in turn may be used to make more robust predictions of corrosion damage in these steels.

2.4 Comparison of the Resistance of Several Steels to Pitting Corrosion

A set of experiments was performed to study the electrochemical and corrosion behavior of steels 20Kh13 and 17-4PH, in order to compare the tendencies of steels with different compositions toward pitting corrosion.

To compare the corrosion resistance of 403SS, A470/471, 20Kh13, and 17-4PH, Table 2-1 lists the corrosion current densities in the pits in 0.1 M NaCl solution with pH = 6 at 20°C (68°F) during the development of the pitting corrosion damage, when E_{corr} is determined by the presence of pits rather than by the passive state.

Table 2-1
The Corrosion Current in a Pit in 0.1 M NaCl Solution for Various Steels

Steel	A-470	403SS	17-4PH	20Kh13
I_{corr} (A/cm^2)	$7x10^{-5}$	$1.8x10^{-6}$	$3.5x10^{-6}$	$1.2x10^{-6}$

From Table 2-1, it follows that for 403SS, 17-4PH, and 20Kh13, the corrosion current densities are virtually identical (within experimental error). However, the dissolution rate of A470/471 is considerably higher. Additional experiments provided further information on this issue. For instance, in spite of close values of the corrosion current densities for 403SS and 17-4PH, examination of the specimen surfaces showed that the corrosion of 17-4PH steel starts somewhat later and develops somewhat slower. This observation points to a higher corrosion resistance of 17-4PH steel. The results presented on Figures 2-28 and 2-29 are also indirect evidence for the higher resistance. It can be seen that 17-4PH steel has a more noble (more positive) corrosion potential than does 403SS, in both the aerated solution and in the solution saturated with oxygen. In accordance with the conclusions made from Table 2-1, it is seen from Figures 2-28 and 2-29 that the corrosion potentials of A470/471 steel are considerably more negative, and correspondingly its corrosion activity is higher.

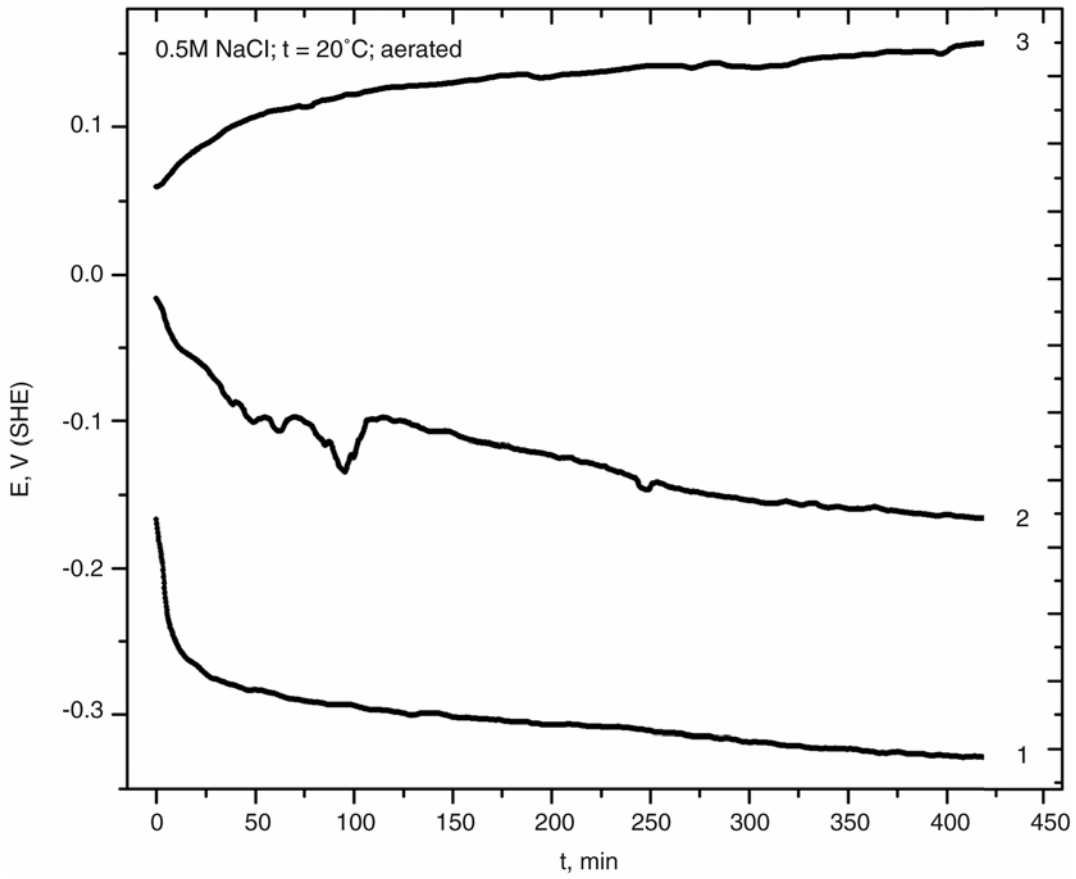

Figure 2-28
Time dependences of the corrosion potentials of A470/471 (Curve 1), 403SS (Curve 2), and 17-4PH (Curve 3) in aerated, 0.5 M NaCl solution.

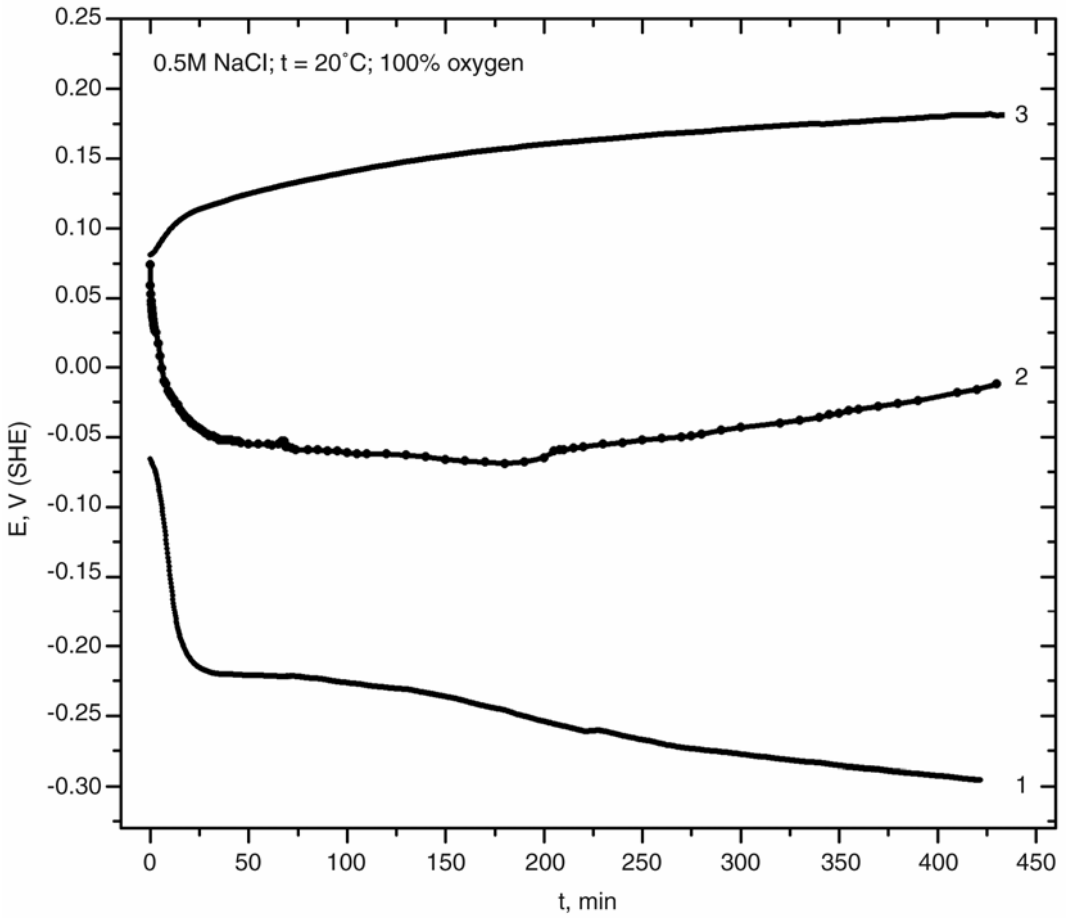

Figure 2-29
Time dependences of the corrosion potentials of A470/471 (Curve 1), 403SS (Curve 2), and 17-4PH (Curve 3) in 0.5 M NaCl solution saturated with oxygen at 20°C (68°F).

3
SUMMARY AND CONCLUSIONS

The findings of this work may be summarized as follows:

1. The quantitative characterization of the principal cathodic partial reactions in the corrosion processes that occur on low pressure steam turbine steels (A470/471 and 403SS) in NaCl solutions of various NaCl concentrations, pH values, temperatures, and dissolved oxygen concentrations is reported.
2. Quantitative dependences of current density for oxygen reduction on dissolved oxygen concentration at temperatures ranging from 20°C to 95°C (68°F to 203°F) and on pH of the solution have been determined. The kinetic equations for oxygen reduction relating the process rate (the current density) to the overpotential of the reaction have also been obtained.
3. The kinetic equations for hydrogen evolution, which proceeds according to two mechanisms—the discharge of hydroxonium ions and the discharge of water molecules—have been developed. The ranges of pH, over which hydrogen evolution proceeds by each of these mechanisms, have been determined.
4. It is shown that the corrosion potential of both steels varies with time as pitting corrosion develops; this may indicate that the corrosion rate of the steels also varies with time.
5. The anodic and cathodic polarization curves on the electrodes totally activated with chloride ion were obtained. Using these data, the corrosion potential and the current density of steel dissolution in the pits has been estimated.
6. The pH values of solution and the concentration of dissolved oxygen have the strongest effect on the corrosion current in a pit. The corrosion current decreases by more than an order of magnitude with an increase in the pH value from 2 to 10 and with a decrease in the concentration of oxygen from 10^{-6} mol/cm^3 (oxygen atmosphere) to 10^{-8} mol/cm^3 (argon atmosphere).
7. On processing of the experimental data, equations predicting the corrosion potential and corrosion current under various conditions were obtained. These equations can be used in the previously developed models and computer codes for predicting corrosion damage in low pressure steam turbines.
8. From the comparison of the experimental data, it may be concluded that the order of resistance to pitting corrosion in NaCl solutions is 17-4PH, steels 403SS and 20Kh13, and steel A470/471, which shows the lowest resistance to pitting corrosion.

4
REFERENCES

1. O. Jonas, *Material Performance*, 24, 9 (1985).
2. T. H. McCloskey, R. B. Dooley, and W. P. McNaughton. *Turbine Steam Path Damage: Theory and Practice*. Electric Power Research Institute, Palo Alto, CA: 1999. TR-108943-V2.
3. G. Engelhardt and D. Macdonald. Development of Code to Predict Stress Corrosion Cracking and Corrosion Fatigue of Low Pressure Turbine Components, EPRI, Palo Alto, CA: 2004. 1004190.
4. G. Engelhardt, D. D. Macdonald, and B. Dooley "Prediction of the Accumulation of Localized Corrosion Damage to Low Pressure Steam Turbines in Fossil Service," *Seventh Intl. Conf. Cycle Chem. Fossil Plants*, Houston, TX, June 3-5, 2003.
5. G. Engelhardt, D. D. Macdonald, Y. Zhang, and B. Dooley, *PowerPlant Chemistry*, 6, 647 (2004).
6. Y. Miyata, S. Asakura, *Corros. Sci.* 44 (2002) 589.
7. R.A.T. De Greef, L.J.J. Janssen, *J. Appl. Electrochem.* 31 (2001) 693.
8. M. Sfaira, A.Shihiri, H. Takenouti, M. Marie de Ficquelmont-Loizos, A. Ben Bachir, M. Khalakhil, *J. Appl. Electrochem.* 31 (2001) 537.
9. N. Le Bozec, C. Compere, M. L'Her, A. Laouenan, D. Costa, P. Marcus, *Corros. Sci.* 43 (2001) 765.
10. V.G. Levich, *Physicochemical Hydrodynamics*, Moscow: Fizmatgiz, 1959.
11. C. Wagner, W. Traud, Z. *Elektrochem.* 44 (1938) 391.
12. A. Turnbull, S. Zhou, *Corros. Sci.* 46 (2004) 1239.
13. M. Duprat, N. Bui, F. Dabosi, *J. Appl. Electrochem.* 8 (1978) 455.

Printed on recycled paper in the United States of America

The Electric Power Research Institute (EPRI)

The Electric Power Research Institute (EPRI), with major locations in Palo Alto, California, and Charlotte, North Carolina, was established in 1973 as an independent, nonprofit center for public interest energy and environmental research. EPRI brings together members, participants, the Institute's scientists and engineers, and other leading experts to work collaboratively on solutions to the challenges of electric power. These solutions span nearly every area of electricity generation, delivery, and use, including health, safety, and environment. EPRI's members represent over 90% of the electricity generated in the United States. International participation represents nearly 15% of EPRI's total research, development, and demonstration program.

Together...Shaping the Future of Electricity

Program:

Boiler Turbine Steam and Cycle Chemistry
Steam Turbines, Generators, and Balance-of-Plant

1010184

ELECTRIC POWER RESEARCH INSTITUTE
3420 Hillview Avenue, Palo Alto, California 94304-1395 • PO Box 10412, Palo Alto, California 94303-0813 USA
800.313.3774 • 650.855.2121 • askepri@epri.com • www.epri.com